Alma Mater Studiorum · University of Bologna

Department of Physics and Astronomy
Department of Biological, Geological and Environmental Sciences

Master Degree in Science of Climate

A New Window into the Oceans: Dynamic Analysis of Sea Level Anomalies from the SWOT mission

Supervisor:
Prof. Paolo Oddo

Co-supervisor:
Dr. Baptiste Mourre

Submitted by:
Martina Auditore

Academic Year 2023/2024

Abstract

Gli eddy mesoscalari rivestono un'importanza cruciale nella dinamica degli oceani, poiché influenzano il trasporto di energia, calore e nutrienti, nonché la circolazione su scala globale. Tuttavia, la loro osservazione presenta notevoli difficoltà a causa della limitata risoluzione spaziale e temporale fornita dall'altimetria tradizionale. La missione Surface Water and Ocean Topography (SWOT), attraverso l'uso dell'altimetria interferometrica a larga banda, offre dati ad una risoluzione senza precedenti per l'analisi di queste strutture. Questo studio valuta il valore aggiunto di SWOT nel Bacino Algerino, una regione caratterizzata da un'intensa attività di eddy. Un'analisi comparativa ha confermato la capacità di SWOT di risolvere la variabilità alle scale più fini e di preservare una maggiore energia alle piccole scale rispetto all'altimetria convenzionale. Lo studio si è concentrato su un eddy anticiclonico costiero, confrontando le osservazioni SWOT con i dati altimetrici convenzionali e i risultati di un modello numerico. SWOT ha permesso di descrivere con maggiore dettaglio la struttura e l'evoluzione dell'eddy, rivelando caratteristiche non risolvibili dai prodotti altimetrici convenzionali, inclusa la fase di dissipazione e la successiva formazione di una nuova struttura. L'analisi combinata dei dati SWOT e dei risultati del modello numerico ha evidenziato il ruolo delle interazioni batimetriche nel processo di dissipazione dell'eddy, attraverso la perdita di vorticità potenziale e l'aumento della componente ageostrofica del moto. Questi risultati dimostrano il potenziale di SWOT nel migliorare la comprensione della dinamica degli eddy e della loro interazione con il fondale oceanico, aprendo la strada a osservazioni oceanografiche ad alta risoluzione sempre più dettagliate.

Abstract

Mesoscale eddies play a fundamental role in ocean dynamics, influencing the transport of energy, heat and nutrients, as well as large-scale circulation. However, their observation remains challenging due to the limited spatial and temporal resolution of conventional altimetry. The Surface Water and Ocean Topography (SWOT) mission, using wide-swath interferometric altimetry, provides unprecedented high-resolution data for studying these structures. This study assesses SWOT's added value in the Algerian Basin, a region characterized by significant eddy activity. A comparative analysis confirmed SWOT's ability to resolve finer-scale variability and retain greater energy at smaller scales compared to conventional altimetry. Focusing on a coastal anticyclonic eddy, SWOT observations were compared with conventional altimetry data and numerical model results. SWOT captured the eddy's structure and evolution with higher precision, revealing previously undetected details, including its dissipation and the subsequent formation of a new structure. The combined analysis of SWOT data and numerical model results highlighted the role of bathymetric interactions in eddy dissipation through potential vorticity loss and increased component of the ageostrophic motion. These findings demonstrate SWOT's potential to enhance our understanding of eddy dynamics and their interaction with the ocean floor, paving the way for improved high-resolution oceanographic observations.

Contents

Chapter 1

Introduction

1.1 Background and Context

1.1.1 General role of eddies and their influence on ocean dynamics

The ocean is in constant motion, shaped by the interaction of currents, waves, and turbulence that extend across great distances. Among the most important features of this dynamic system are eddies, which are rotating bodies of water spanning a wide range of spatial and temporal scales. Eddies can vary in size, from a few kilometers to hundreds of kilometers in diameter, and may persist for days, weeks, or even months. Depending on their formation mechanisms and surrounding ocean conditions, they can be highly transient and short-lived or quasi-stationary, remaining in a fixed region for extended periods. Among these, mesoscale eddies (with diameters typically ranging from 50 to 300 km) are the most prevalent and influential. They play a fundamental role in the transport of energy, heat, nutrients, and other physical properties, such as carbon and phytoplankton. They also have a crucial part in regulating climate and mixing

the ocean, directly influencing large-scale ocean circulation patterns (Fu et al. [2010]). Mesoscale eddies are often generated by instabilities of the larger-scale circulation, by the interaction of ocean currents with irregular seafloor topography, and in some cases, due to direct atmospheric forcing (Poulain et al. [2021], Stammer et al. [2001]). Once formed, these eddies can last from weeks up to several months, propagating over considerable distances.

They are categorized as cyclonic or anticyclonic, depending on their rotation. In the Northern Hemisphere, cyclonic eddies (anticlockwise) are associated with the upwelling of deeper, cooler water, resulting in a cold core that influences the thermocline by inducing an upward displacement. In contrast, anticyclonic eddies (clockwise) trap warmer surface waters, creating a warm core and a downward displacement of the thermocline, enhancing ocean stratification. Their vertical extent is highly variable, ranging from shallow surface-intensified structures to deep eddies that can extend well below the thermocline. In the latter case, they can significantly alter the vertical thermal structure of the ocean, influencing deep water circulation and mixing processes.

One of the key roles of mesoscale eddies is their broader impact on ocean circulation and climate. Recent studies have profoundly redefined the traditional view of ocean circulation, pointing out the active role of mesoscale eddies in shaping the variability of the global ocean. Lozier [2010] challenged the classic "conveyor belt" model of the Meridional Overturning Circulation (MOC), suggesting that eddies significantly disrupt and redefine ocean transport pathways. Unlike the previously assumed continuous flow of water masses, the MOC is now seen

as a complex network where eddies and regional variability play central roles in regulating the exchange of energy and materials. Zhang et al. [2014] further illustrated the magnitude of eddy influence, quantifying the eddy-induced zonal mass transport as reaching up to 30-40 Sverdrups ($1Sv = 10^6 m^3/s$) in subtropical regions. This transport is comparable to that driven by large-scale wind and thermohaline circulation, highlighting the role of mesoscale eddies as transporters of heat, carbon, and biogeochemical tracers.

Additionally, mesoscale eddies significantly influence marine ecosystems by redistributing nutrients and microorganisms, which enhances primary productivity and supports biogeochemical cycles (Chelton et al. [2011]). For instance, cyclonic eddies enhance productivity by upwelling nutrient-rich deep water, promoting plankton growth, and providing important feeding grounds for marine life. Anticyclonic eddies, meanwhile, influence water column stratification, affecting nutrient availability and vertical mixing. This dual role makes eddies central to biogeochemical cycles and resource distribution.

1.1.2 Overview of the Algerian Basin

The Mediterranean Sea is a semi-enclosed basin characterized by complex circulation patterns, strong evaporation-driven salinity gradients, and highly heterogeneous bathymetry. Its hydrodynamics are shaped by water exchanges with the Atlantic Ocean through the Strait of Gibraltar, as well as the presence of numerous mesoscale eddies. These eddies interact closely with regional dynamics, heavily influenced by the constrained basin geometry and complex bathymetry (Robinson et al. [2001]). In particular, coastal eddies, that form and evolve near the coast, are

especially affected by bathymetry, making them very relevant in the Mediterranean Basin.
The Algerian basin, located in the southern part of the Western Mediterranean Sea (WMed), is a dynamic oceanographic region that extends from the coast of Algeria and is limited by the Balearic Islands to the north and the Sicilian Channel to the east (fig.1.1.1). This relatively small basin is characterized by both basin-scale and mesoscale dynamics.

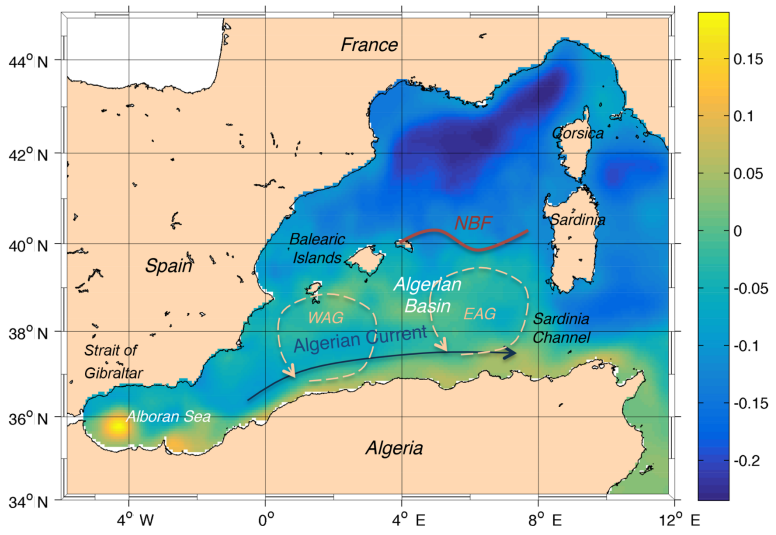

Figure 1.1.1: Mean dynamic topography (m) in the WMED (Rio et al. 2014). The plot shows the Eastern Algerian Gyre, the Western Algerian Gyre (dashed yellow circles) and the Algerian Current (blue arrow).

At the surface, the mean circulation is dominated by the Algerian current, that flows along the African coast at several tens of centimeters per second (Pinardi and Masetti 2000). This current, made of Atlantic Water (AW), enters the Mediterranean through the Gibraltar Strait, compensating for the deficit of water due to evaporation. After the Greenwich meridian, the current becomes shallower and wider near the Sardinia Channel

(Millot [1985], Fusco et al. [2008]). This water mass gradually transforms into Modified Atlantic Water (MAW) as it flows eastward. Below the surface, Testor et al. [2005] described the subsurface circulation using Lagrangian floats and deep current meters, revealing the presence of two large anticyclonic gyres, known as the Algerian Gyres (fig. 1.1.1). These gyres, largely barotropic, follow the f/H contours (where f is the planetary vorticity and H is the depth), indicating that their dynamics are strongly constrained by the bathymetry (Escudier et al. [2016]). The Levantine Intermediate Water (LIW) participates in shaping the basin's subsurface circulation (fig. 1.1.2). LIW formation occurs over much of the Levantine basin, but preferentially in the north, probably due to meteorological factors (Robinson et al. [2001]).

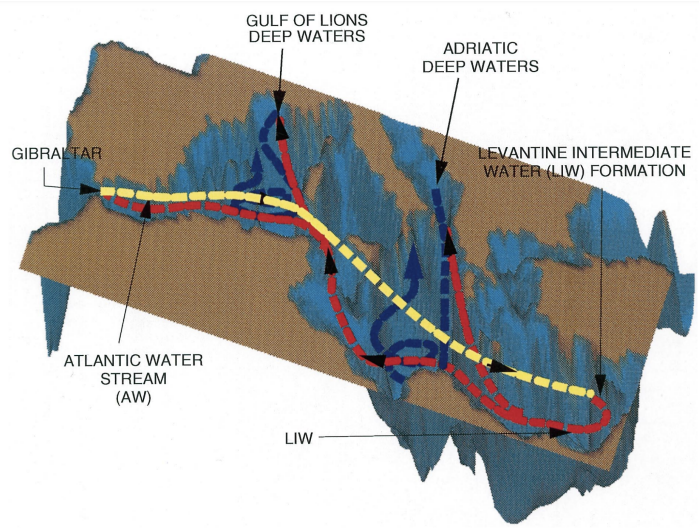

Figure 1.1.2: The schematic of the thermohaline circulation in the basin with the major conveyor belt systems indicated by dashed lines with different colors. The yellow indicates the AW stream, the red indicates the mid-depth LIW and the blue lines indicate the meridional cells induced by deep waters (Pinardi and Masetti [2000]).

It flows westward through the Sicily Channel, entering the Western Mediterranean at intermediate depths (200–500 m), following bathymetric contours and facilitating the exchange of heat and salt between the eastern and western Mediterranean basins (Pinardi and Masetti [2000]). The LIW layer was found to play an important role in deep-water formation sites (Gulf of Lions), affecting the formation processes. Finally, LIW contributes predominantly to the outflow from Gibraltar to the Atlantic Ocean. (Robinson et al. [2001]).

At greater depths, the Western Mediterranean Deep Water (WMDW), formed in the Gulf of Lions (fig. 1.1.2), flows southward into the Algerian Basin, interacting with the basin's topography and contributing to vertical mixing processes and where it takes part in the outflow of Mediterranean water into the Atlantic Ocean (Pinardi and Masetti [2000]).

The circulation in the Algerian Basin exhibits both seasonal and interannual variability, driven primarily by wind forcing and thermohaline gradients. Seasonal changes modulate the strength of the Algerian Current, which in turn influences mesoscale activity. During winter, stronger winds and enhanced baroclinic instabilities enhance the formation of energetic meanders and eddies. In contrast, summer conditions, characterized by weaker winds and stronger stratification, tend to stabilize the current, reducing the intensity of mesoscale variability (Pinardi and Masetti [2000]). At interannual timescales, variability in wind stress and heat fluxes significantly affects the circulation structure and eddy activity within the Algerian Basin. Changes in atmospheric forcing can alter the strength and pathways of the Algerian Current and variations in wind stress amplitude have been identified as a key driver of circulation changes at

longer timescales (Pinardi and Masetti [2000]).
The Algerian basin's mesoscale variability is characterized by baroclinic instabilities of the Algerian Current, that cause meanders and eddies, that often detach from the main flow and propagate into the open basin (Millot [1999], Obaton et al. [2000]). These features play a key role in the redistribution of heat, salinity, and nutrients over large distances, significantly influencing the physical and biogeochemical processes in the basin (Escudier et al. [2016]). Detailed analyses of mesoscale features will be addressed in the subsequent section.

1.1.3 Algerian current and mesoscale eddies in the Algerian basin

The Algerian Current is the main feature of surface circulation in the Algerian Basin. It transports Atlantic Water, highly modified by upwelling and mixing processes, and is thus referred to as Modified Atlantic Water (Millot [1999]). At 0°E, the Algerian Current has a width of approximately 50 km, a maximum depth of about 150 m, and a mean velocity of 30 cm/s, with maximum values reaching 50 cm/s. It then becomes wider and shallower further east, particularly around the Sardinia Channel (Fusco et al. [2008]). The current is baroclinically unstable and often forms meanders and mesoscale eddies. These eddies, known as Algerian Eddies (AEs), can reach diameters of 50–150 km and include both cyclonic and anticyclonic structures. AEs propagate eastward along the North African coast, persisting for weeks or even months. The mean propagation velocity of these eddies has been measured at approximately 3–4 cm/s (Escudier et al. [2016], Pessini et al. [2018]).
Seasonal variability plays a significant role in modulating the

intensity of the Algerian Current and its associated mesoscale structures. During winter, stronger wind stress and reduced stratification enhance baroclinic instabilities, leading to the formation of more energetic eddies. Conversely, in summer, weaker winds and increased stratification reduce the intensity of eddy generation (Pinardi and Masetti [2000]).
The formation of AEs occurs in three main areas (fig 1.1.3):

- Region between 2°W to 1°W: this is the strongest eddy formation zone, generating structures that propagate eastward along the coast.
- Region between 1°E to 3°E: this is a weaker formation area for eddies.
- Region between 6°E to 7°E: this is on the eastern part of the eastern Algerian gyre, producing eddies that either stay in this position or detach northward to recirculate around the western Algerian gyre.

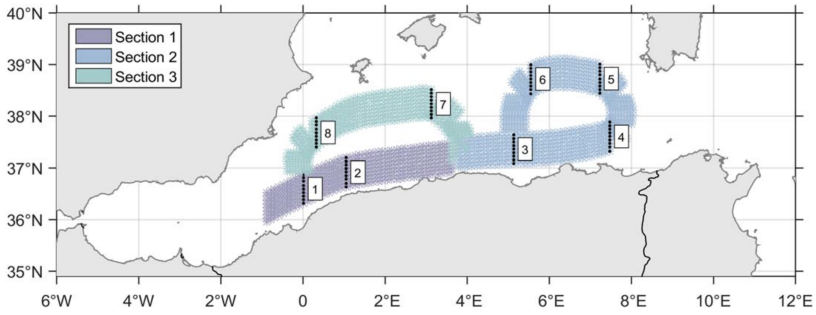

Figure 1.1.3: The three sections corresponding to the different mean eddy pathways (Escudier et al. [2016]).

There are two main propagation patterns for anticyclonic AEs, corresponding to the mentioned barotropic Algerian gyres, as

shown in figure 1.1.3. Eddies generated in the western part of the basin are advected along the first section (near the coast) until they reach 4°E. At this point, they either continue eastward into the eastern Algerian gyre (section 2) or move northward along section 3, recirculating around the western Algerian gyre (Escudier et al. [2016]). These propagation patterns and their spatiotemporal variability are further highlighted in the Hovmöller diagram (fig. 1.1.4). The diagram illustrates the sequence of sea level anomalies (SLA) along the three sections, with red areas indicating strong anticyclonic structures. Section 1 captures the formation of eddies near 1°W, while sections 2 and 3 depict their eastward propagation and subsequent recirculation. This visualization emphasizes the periodic nature of AE formation.

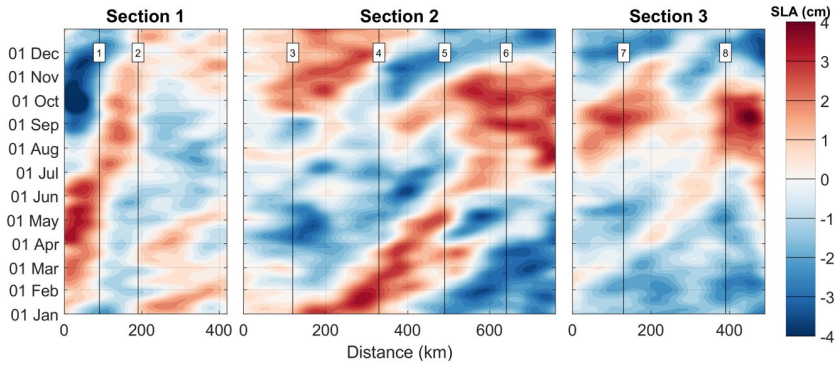

Figure 1.1.4: Annual climatology of the SLA for the period 1993–2014 along the sections indicated in figure 1.1.2 with relevant positions indicated with their number (Escudier et al. [2016]).

In addition, mesoscale eddies in the Algerian Basin exhibit significant variability in their vertical extent, influenced by their origin and interaction with the surrounding environment. Coastal eddies, which often form as meanders of the Algerian Current, typically influence the MAW layer, extending from the surface to

depths of approximately 100–300 meters (Benzohra and Millot [1995]). However, as these eddies detach from the Algerian Current and evolve into open-sea eddies, their vertical influence can often increase. Observations of open-sea AEs show that they can extend beyond 800 meters (Benzohra and Millot [1995]), with signatures of weak anticyclonic rotation detected even at depths of 1000 meters (Ruiz et al. [2002]). While these deeper eddies demonstrate the potential for significant vertical influence, not all AEs penetrate such depths. For instance, an eddy analyzed by Poulain et al. [2021] exhibited a clear vertical extent of 250 meters, with diminishing influence below this depth. Similarly, Escudier [2014] reported that most eddies in the Algerian region have depths shallower than 400 meters, even in areas where deeper eddies have been observed. The depth distribution is centered around 200 meters, highlighting the predominance of relatively shallow structures in the basin.

The properties of mesoscale eddies also depend on their polarity and lifetime. Anticyclonic eddies are typically larger and thicker than cyclonic ones, with long-lived structures displaying a significant increase in both average diameter and thickness (Bonaduce et al. [2021]). However, the eddy population decreases significantly when considering long-lived structures, which represent only 20% of the total mesoscale eddies in the basin (Bonaduce et al. [2021]).

Overall, mesoscale eddies, with their variability, propagation, and interaction with water masses, play a fundamental role in shaping the dynamics and energy distribution of the Algerian Basin.

1.2 Conventional Altimetry: an overview

1.2.1 Fundamentals of Conventional Altimetry

The dynamics of mesoscale eddies have been a central theme of physical oceanography research for many years. The advent of Earth-observing satellites in the late 1970s revolutionized the field by providing unprecedented opportunities to study these phenomena on a global scale. Since then, satellite altimetry has proven to be a powerful tool to investigate mesoscale phenomena, offering an opportunity to study the temporal and spatial variability of eddies at a level of detail previously unavailable (Fu et al. [2010]).
Altimetry-dedicated satellites are equipped with sensors, which usually transmit microwave pulses in the radar frequency domain to Earth's surface and measure the travel time of radar pulses reflected from the ocean surface. This travel time is then used to determine the range, i.e. the distance between the satellite and the sea surface. To derive the absolute sea surface height (SSH), the position of the satellite must also be known accurately. The SSH is then obtained by subtracting the range from the satellite's orbital altitude (h_{sat}) (fig. 1.2.1):

$$SSH = h_{sat} - range$$

However, the absolute sea surface height alone does not provide direct information about ocean variability. To extract meaningful oceanographic signals, the SSH needs to be referenced to the geoid, which represents the Earth's gravitational equipotential surface. Additionally, the Mean Dynamic Topography (MDT)—the long-term mean deviation of SSH from the geoid

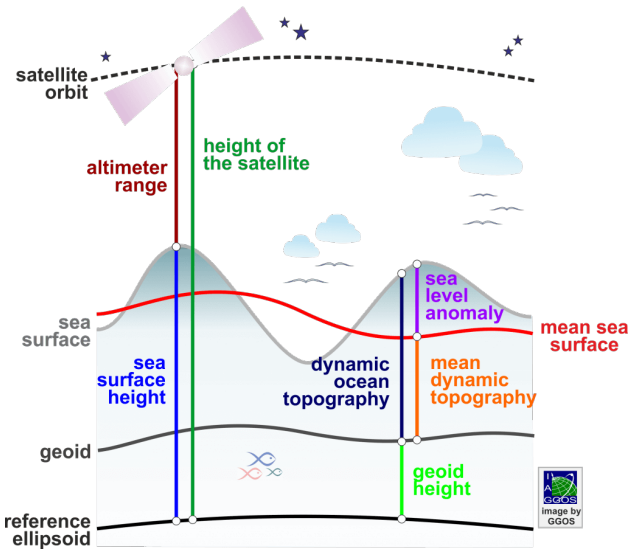

Figure 1.2.1: Definition of various quantities related to sea-surface-heights, including MDT, SSH and SLA. The geoid is also depicted in the picture (from Global Geodetic Observing system).

due to ocean circulation—must be subtracted to obtain Sea Level Anomaly (SLA) (fig. 1.2.1):

$$SLA = SSH - Geoid - MDT$$

To ensure accurate SLA measurements, a series of geophysical and instrumental corrections must be applied. These corrections serve different purposes, addressing environmental influences, instrumental biases, and data processing requirements. They include:

- Dynamic Atmospheric Correction (DAC), which removes the effects of atmospheric variability on sea level, including the impact of atmospheric pressure variations and the response of the ocean to wind-driven forcing. In conventional altimetry, DAC is typically performed using the MOG2D-

G (2 Dimension Gravity Waves) model, developed by LEGOS/CNRS, which is specifically designed to correct high-frequency atmospheric signals (periods shorter than 20 days). For lower-frequency atmospheric influences, an inverted barometer correction is applied, assuming a static ocean response to atmospheric pressure changes.

- Corrections for ocean barotropic and internal tides to eliminate periodic vertical displacements of the sea surface. These corrections ensure consistency between tracks.

- Long-wavelength error correction to compensate for instrumental drift and biases.

SLA data are initially processed as Level-2 and Level-3 products (respectively, single and multiple tracks), which consist of pointwise measurements collected along satellite tracks. However, a major limitation of these datasets is that they are not synoptic, meaning different regions of the ocean are sampled at different times depending on the satellite's orbit. To overcome this, Level-4 products are generated by merging multiple altimetric datasets over a ±6-week temporal window. This process involves several filtering techniques, such as the removal of tides and wind-driven variability, followed by optimal interpolation, which fills data gaps and smooths spatial variability to produce gridded SLA fields. While the nominal along-track resolution of conventional altimeters depends on the sampling frequency, most missions operate at a 1 Hz rate, corresponding to an approximate spatial resolution of 6–7 km (exact values depend on latitude). More recent datasets, such as those available at 5 Hz, provide a nominal resolution of about 1 km. However, despite this fine-scale sampling, the effective resolution of gridded

SLA products is significantly lower due to post-processing filters applied to reduce noise and ensure data consistency. These filters, while necessary for improving data quality, constrain the physical signal resolvable in SLA fields to larger spatial scales, typically around 50–70 km. This limitation is particularly relevant when studying energetic eddy fields, such as those in the Algerian Basin.

Another critical limitation of conventional altimetry is its reduced performance in coastal regions (Aulicino et al. [2018]). The radar altimeter onboard satellites is designed to measure sea level based on the reflection of microwave pulses from the ocean surface. However, in coastal areas, the presence of land introduces land-sea contamination, which degrades the quality of the altimetric signal. This leads to data gaps near the coastline, where sea level measurements become unreliable or entirely unavailable. The inability to measure SSH accurately in these regions presents significant challenges for the study of coastal mesoscale processes. In the Algerian Basin, where coastal dynamics play a significant role in mesoscale variability, this limitation is particularly critical. Coastal eddies, which form as instabilities of the Algerian Current and often propagate along the continental slope, can be challenging to monitor with conventional altimetry. The inability to capture sea-level variations close to the coast limits the understanding of their formation mechanisms and their interaction with the larger circulation.

Nevertheless, despite these constraints, conventional satellite altimetry has played a crucial role in advancing our understanding of mesoscale eddy dynamics across the Mediterranean Sea.

1.2.2 State of the art of monitoring eddies with Conventional Altimetry in the Algerian Basin

The application of conventional altimetry has been crucial in advancing our understanding of mesoscale dynamics. In the Algerian Basin, these observations have provided valuable insights into the formation, evolution, and pathways of eddies. The following section reviews key studies that have used altimetric data to investigate these processes

The main altimetric missions covering this region include the Sentinel series, Jason series, Topex/Poseidon, Saral/AltiKa, and Cryosat-2, which have provided consistent datasets spanning multiple decades. Over the years, these altimetric datasets have been fundamental in studying Algerian Eddies, which are key drivers of regional circulation and heat transport.

Font et al. [2004] demonstrated the potential of conventional altimetry to monitor mesoscale eddies by analyzing a large anticyclonic eddy (AE 98-1) in the Western Mediterranean. They applied the Okubo-Weiss criterion to the SLA data, a widely used method to identify and characterize mesoscale eddies based on the relative dominance of vorticity and strain rate in a given region. This criterion is defined as:

$$W = s_n^2 + s_s^2 - \omega^2$$

where s_n^2 and s_s^2 are the normal and shear components of the strain rate tensor, respectively, and ω is the relative vorticity. A negative value of W indicates that vorticity dominates over strain, identifying a coherent eddy structure, whereas a positive value suggests strain-dominated regions, where the flow is more deformative and less coherent. Using this approach, they identified the core of the anticyclonic eddy and successfully tracked

its evolution over time. The eddy, with a diameter of approximately 140 km, moved eastward at a speed of about 3 cm/s, while the maximum tangential velocities (i.e. the speed of fluid parcels moving along circular trajectories around the eddy core) reached 40–50 cm/s. The integration of altimetric data with Lagrangian drifter observations validated the reliability of altimetry in capturing the structure and dynamics of mesoscale eddies, even in the absence of strong surface temperature or ocean-color gradients.

Escudier et al. [2016] made substantial contributions to the comprehension of the Algerian Basin through an extensive analysis of over 20 years of satellite altimetry data. Their work employed advanced eddy detection methods and cross-correlation analysis to reveal key properties of Algerian Eddies, such as their size, structure, propagation paths, and variability. Their findings revealed that AEs exhibit diameters between 50 and 150 km and propagate eastward at speeds of 3–4 cm/s, before detaching from the Algerian Current, following pathways dictated by the barotropic gyres in the Algerian Basin (fig. 1.1.3). They also highlighted the significant seasonal and interannual variability in AEs formation and propagation.

Pessini et al. [2018] extended this analysis by incorporating 24 years of altimetric data (L4 gridded product), using improved automatic detection and tracking methods based on SLA and the Okubo-Weiss parameter. These techniques allowed for the identification of key properties such as eddy lifespan, kinetic energy, and trajectories. Their study revealed distinct pathways for cyclonic and anticyclonic eddies and demonstrated that anticyclonic eddies contribute more significantly to mesoscale circulation. Additionally, the study emphasized the value of altime-

try to overcome the limitations of other observational methods, such as infrared imagery and ocean color data, which are often hindered by cloud cover.

Mesoscale eddies not only dominate the sea surface height variability in the Mediterranean at timescales beyond one month but also drive a significant portion of the ocean's kinetic energy, with contributions exceeding 50–60% both at the surface and at depth (Bonaduce et al. [2021]). These insights underscore the critical role of long-term satellite altimetry datasets in advancing our understanding of mesoscale dynamics, especially in capturing the evolution of anticyclonic and cyclonic structures in regions like the Algerian Basin. As highlighted by Zhang et al. [2014], eddy-induced mass transport is comparable in magnitude to the large-scale wind and thermohaline-driven circulation, emphasizing their importance as transporters in global ocean dynamics. These processes, captured extensively through altimetric measurements, provide a critical foundation for interpreting the physical and biogeochemical variability of the Mediterranean Sea.

Overall, conventional altimetry stands out for its ability to deliver global coverage and provide consistent spatial and temporal data over decades. This comprehensive approach has been essential for understanding the role of Algerian Eddies in shaping the basin's circulation and energy transport.

Despite inherent limitations, particularly in resolving finer-scale features and near-coastal processes, the contribution of conventional altimetry to the study of mesoscale variability remains central. Its extensive data records continue to serve as a robust foundation for advancing oceanographic research on both regional and global scales.

1.2.3 Limits and weaknesses of present altimetric products

Despite the significant contributions of conventional altimetry to oceanographic research, several limitations affect its ability to fully capture ocean variability, particularly in coastal and high-energy regions, as already mentioned in the previous sections.

- The spatial resolution is significantly lower than the nominal sampling rate due to post-processing filters applied to reduce noise. These filters constrain the smallest resolvable physical signals to scales of approximately 50–70 km, limiting the ability to detect smaller mesoscale and submesoscale features.

- The temporal resolution of conventional altimetry is constrained by the satellite's revisit time over the same location. For example, the Jason series covers the same location approximately every 10 days, which is sufficient for detecting larger, slower mesoscale features but inadequate for capturing rapid variations in ocean dynamics. High-frequency events, such as the formation or dissipation of eddies, are often undersampled. This leads to incomplete data on their life cycles, interactions with coastal currents, and their energetic contributions to the basin's dynamics.

- Conventional altimetry experiences significant performance degradation near the coast due to land-sea contamination, leading to data gaps and reduced measurement accuracy. This limitation is particularly relevant in the Algerian Basin, where coastal eddies form and evolve along the continental slope. The lack of reliable sea level observations in these

areas restricts the ability to study eddy-coastal current interactions and their influence on regional circulation.

These limitations highlight the need for complementary observational tools to fill the gaps left by conventional altimetry. Poulain et al. [2021] and Bonaduce et al. [2021] emphasized the importance of integrating satellite altimetry with in-situ measurements, such as Argo floats and drifters, to provide a more detailed and comprehensive view of ocean dynamics. This multiplatform approach enhances our ability to monitor mesoscale and coastal processes, particularly in regions like the Algerian Basin, where coastal features challenge traditional observation methods.

Alongside these methods, the Surface Water and Ocean Topography (SWOT) mission introduces a new altimetric approach based on wide-swath interferometry, which overcomes many of the limitations of conventional altimetry. Unlike traditional nadir altimeters that provide only along-track measurements, SWOT delivers two-dimensional SSH fields at 1 km resolution over a 120 km-wide swath (fig. 1.2.2). This allows for a more detailed representation of mesoscale and submesoscale variability (Morrow et al. [2019]), particularly near the coast, where SWOT provides improved data continuity compared to conventional missions. By offering higher spatial resolution and enhanced coastal coverage, SWOT is expected to significantly improve our understanding of fine-scale ocean features, such as eddies and fronts, and their role in regional circulation. A key component of the mission was the fast-sampling phase, which took place in the first months after launch. During this phase, SWOT operated on a 1-day repeat orbit, allowing for an unprecedented temporal resolution of mesoscale and submesoscale processes.

Further details on SWOT's data and processing methods are provided in section 2.1.

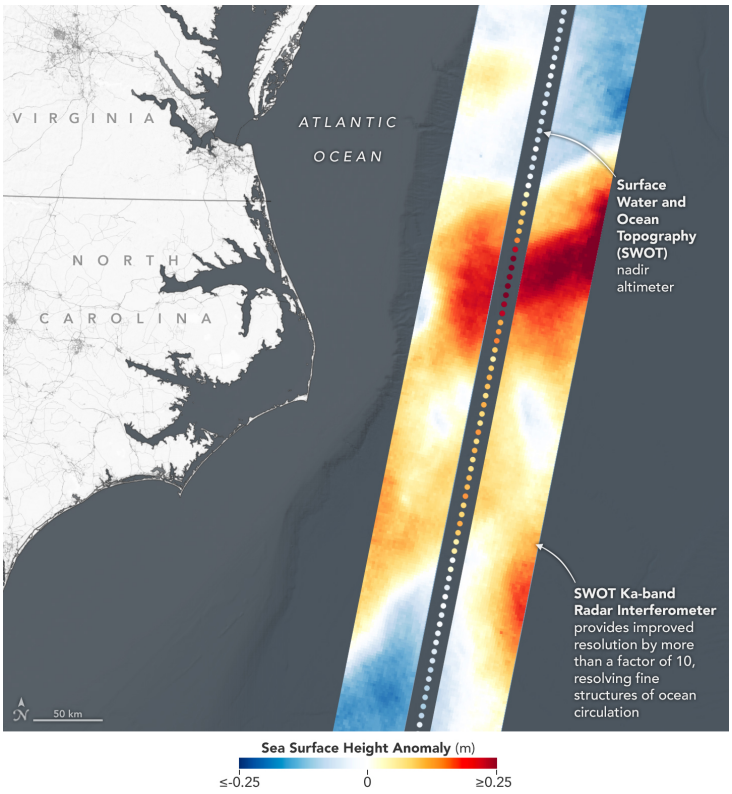

Figure 1.2.2: Schematic of the SWOT measurements showing the area covered by the interferometers and the nadir altimeter.

1.3 The role of modeling in ocean observation and monitoring

Numerical models complement observations, providing a more comprehensive picture of ocean processes. While satellite altimetry delivers crucial SSH data, it is inherently limited by spatial and temporal sampling constraints. Numerical simula-

tions help bridge these gaps by offering a continuous, three-dimensional representation of ocean dynamics, enabling the study of processes that are difficult to observe directly, such as sub-surface circulation and mesoscale eddy interactions with bathymetry.
Operational ocean forecasting systems, such as the Mediterranean Forecasting System (MFS, Pinardi et al. [2002], Pinardi and Coppini [2010]), play a crucial role in improving ocean monitoring. These high-resolution models assimilate satellite and in-situ observations to generate daily ocean state estimates. The resulting forecasts and reanalysis datasets, provided by the Copernicus Marine Service (CMEMS), offer valuable insights into mesoscale and submesoscale variability, including the formation, evolution, and dissipation of eddies, as well as their influence on regional circulation and stratification patterns.
By complementing SWOT data with numerical simulations, it is possible to gain a more detailed representation of mesoscale eddies, assessing their structure, evolution, and interaction with bathymetry. This multi-source approach enhances the ability to evaluate the consistency of SWOT observations, refine the interpretation of altimetric data, and provide a more comprehensive understanding of the processes governing mesoscale variability in the Mediterranean Sea.

1.4 Objective of the work

This work focuses on the evaluation and quantification of the added value of the SWOT mission in capturing mesoscale and studying coastal dynamics, particularly in the Algerian Basin. The primary objective is to assess whether SWOT improves the study of small-scale coastal eddies compared to conventional

satellite altimetry. To this end, we analyze the same eddy using both SWOT and conventional altimetry, comparing their ability to resolve its structure, propagation, and interaction with the surrounding circulation. In addition to satellite altimetry, this study integrates other remote sensing data, such as Sea Surface Temperature (SST) and Ocean Color (OC) maps, to provide complementary information on eddy-related processes.
To deepen the analysis, this study incorporates the use of numerical models primarily as a tool for supporting the interpretation of SWOT observations. These models help to better understand the mesoscale features detected by SWOT and to analyze the three-dimensional structure and dynamics of eddies, particularly in relation to their interaction with bathymetry.
The choice of the Algerian Basin as the study area is motivated by its frequent mesoscale activity and its position as a selected site for daily repeated tracks during the SWOT fast-sampling phase. The southern region of Mallorca, in particular, serves as an ideal focus due to the frequent formation and propagation of eddies in this area (fig. 1.4.1). This study also benefits from the expertise and resources of IMEDEA (Instituto Mediterráneo de Estudios Avanzados), a leading research center in ocean and coastal dynamics.
In summary, the objectives of this work are:

- To validate the reliability and performance of SWOT data.
- To highlight the improvements provided by SWOT altimetry by comparison with conventional altimetry in resolving mesoscale dynamics.
- To study the eddy characteristics and interactions with bathymetry.

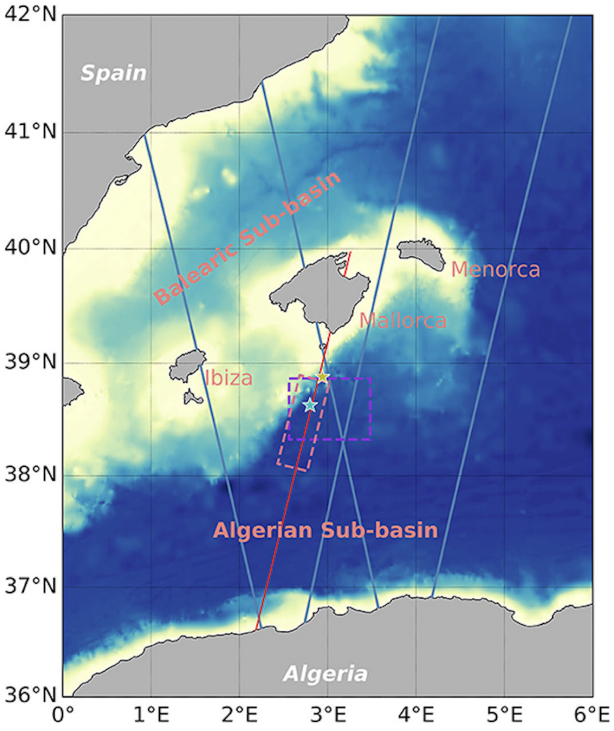

Figure 1.4.1: Limits of SWOT swaths in the Western Mediterranean during the fast-sampling phase.

Chapter 2

Data

This chapter provides an overview of the datasets used in this study. The datasets analyzed include SWOT data, conventional altimetry, sea surface temperature, ocean color observations, and numerical model outputs. Each dataset contributes to different aspects of the analysis, providing essential information for the study of mesoscale eddies in the Algerian Basin.

2.1 SWOT

The Surface Water and Ocean Topography (SWOT) mission, launched in December 2022 as a joint effort between NASA (National Aeronautics and Space Administration) and CNES (Centre National D'Études Spatiales), aims to overcome the longstanding limitations of conventional altimetry, discussed in the previous paragraph. By combining traditional nadir altimetry with innovative wide-swath interferometry, SWOT enables the acquisition of two-dimensional SSH data at an unprecedented resolution of 1 km, over a 120 km wide swath (fig. 1.2.2) (d'Ovidio et al. [2019]).
The mission is driven by two primary scientific objectives (Fu

et al. [2012]). The first, which is directly relevant to this work, focuses on providing high-resolution measurements of ocean surface topography, to improve the understanding of oceanic mesoscale and submesoscale processes. The second, beyond the scope of this study, involves measuring water elevation on land, to study the spatial and temporal distribution of water storage and discharge.

To achieve these objectives, SWOT carries two complementary instruments: a conventional nadir altimeter and the Ka-band Radar Interferometer (KaRIn). The nadir altimeter operates at 1 Hz (7 km resolution along-track), similar to Jason-3 and Sentinel-3, and can also function at 20 Hz (350 m along-track resolution), which enhances coastal and inland water monitoring. However, the key innovation of SWOT is KaRIn, a radar interferometer with two antennas spaced 10 meters apart, enabling precise wide-swath SSH measurements on both sides of the nadir track. This setup allows for the first-ever direct synoptic observations of ocean topography in two dimensions (Fu et al. [2024]), with an effective spatial resolution of 15–30 km in wavelength, depending on sea state (Morrow et al. [2019]).

As discussed in Section 1.2, while conventional altimetry has provided long-term global coverage of sea level change, its limited spatial resolution—particularly near the coasts—remains a significant constraint. SWOT's innovative measurement approach, combining high-resolution along-track sampling with wide-swath interferometry, is designed to enhance our understanding of fine-scale ocean features such as eddies and fronts (Fu et al. [2024]). Furthermore, KaRIn's ability to measure SSH independently of atmospheric conditions, such as cloud cover (d'Ovidio et al. [2019]), significantly improves studies of coastal

processes, inland water bodies, and their interactions with the global climate. Additionally, SWOT's fine-scale SSH data provide a more precise quantification of energy transfers across spatial scales, particularly in regions dominated by mesoscale and submesoscale dynamics, such as the Algerian Basin (Morrow et al. [2019]).
The mission comprises two distinct temporal phases (https://swot.jpl.nasa.gov/).

- Fast-Sampling Phase (March–July 2023): This calibration and validation phase featured a 1-day repeat orbit at 857 km altitude over specific tracks. It focused on achieving calibration objectives and evaluating error spectra through comparisons with independent in situ observations. This phase also demonstrated SWOT's capability in capturing rapidly evolving ocean features, such as submesoscale fronts and eddy formation, which are often undersampled by conventional altimetry.

- Nominal Orbit Phase (after July 2023): SWOT shifted to a 21-day repeat orbit at an altitude of 891 km, enabling long-term observations that will continue for several years.

To ensure accuracy in the measurements, the L3 SWOT product applies several essential geophysical corrections (https://www.aviso.altimetry.fr). Among the key corrections are:

- Dynamic Atmospheric Correction: The MOG2D model, as in conventional altimetry, is employed to account for atmospheric pressure and wind effects on the sea surface. This correction includes the inverted barometer effect and high-frequency atmospheric phenomena.

- Ocean tides: The FES2022 (Finite Element Solution 2022) (Carrere et al. [2022]) model is used to calculate the geocentric ocean tide height. This includes the total ocean tide, load tide, and equilibrium long-period tides. This correction is critical for eliminating tidal signals from the sea surface height anomaly.

- Internal tides: The correction for internal tides uses the HRET (High-Resolution Empirical Tide) (Carrere et al. [2021]) model for coherent tidal frequencies (M2, K1, S2, O1). This is particularly important for removing internal tide signals, improving the quality of SSHA data, and enabling better detection of mesoscale ocean features.

In addition to these key corrections, several other instrumental and geophysical adjustments are applied to improve data quality. These include corrections for propagation delays caused by the wet and dry troposphere and the Sea State Bias correction, to mitigate errors introduced by wave conditions that influence radar pulse reflection.
For the objective of this study, the Level-3 SWOT product was selected, as it provides ocean topography measurements obtained from both the KaRIn interferometric swaths and the nadir altimeter. The dataset includes SSH measurements from KaRIn swaths on both sides of the image, while the nadir altimeter samples the central region, at a lower resolution. The most recent dataset version (v1.0) was used as the reference for all analyses. Among the available variables in the L3 product, we selected the denoised SSHa, which undergoes an AI-based noise reduction process. This filtering technique, conceptually analogous to long-pass filtering in conventional altimetry, reduces

high-frequency instrumental noise while preserving mesoscale signals. Figure 2.1.1 shows an example of the difference between the raw SSHa and the denoised SSHa.

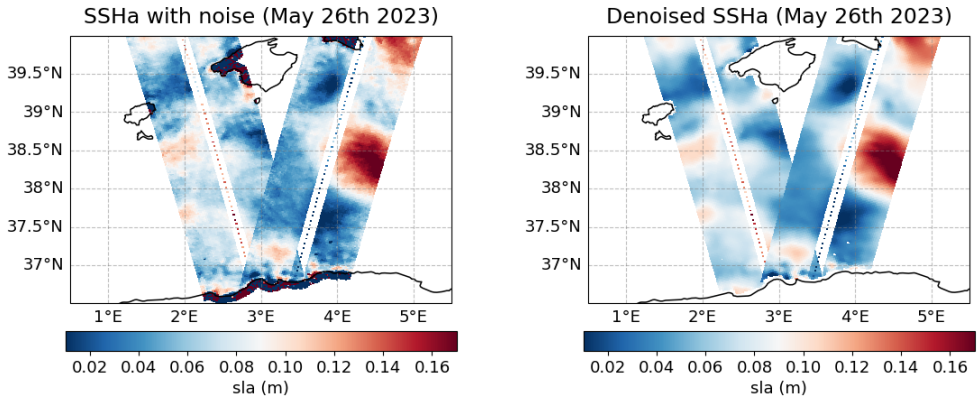

Figure 2.1.1: SSHa with and without noise from SWOT L3 product.

2.2 Conventional Altimetry

For the objective of this study, conventional altimetry maps were used to preliminarily identify eddy features. The analysis used both L3 along-track and L4 gridded altimetry products, both in the reprocessed versions (downloaded from Copernicus Marine Service).
The period selected for this analysis was specifically during the SWOT fast-sampling phase, with a focus on the months of May and June 2023. An example of a SLA map from the L4 gridded product is given in figure 2.2.1.

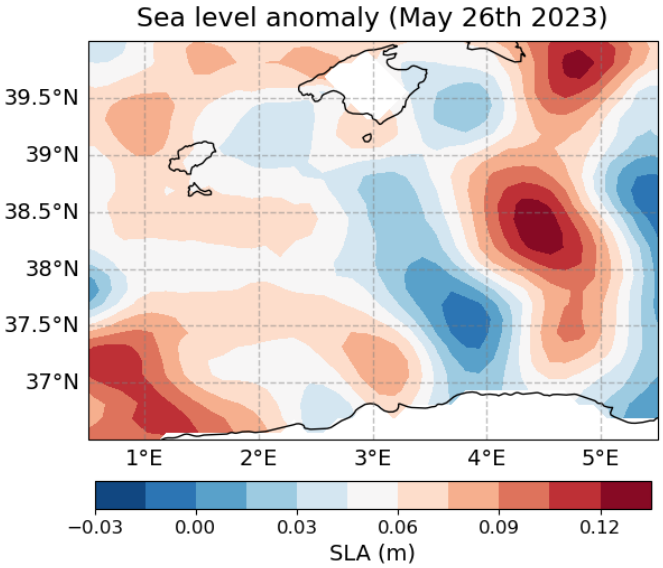

Figure 2.2.1: SLA map of the Algerian Basin from conventional altimetry data (May 26th 2023).

2.3 Sea Surface Temperature

Sea surface temperature (SST) represents a valuable tool for identifying mesoscale structures and, in the context of this study, is primarily used for qualitative assessments.
For this analysis, the L4 Ultra-High Resolution Mediterranean product (Buongiorno Nardelli et al. [2013]) was initially considered. It has a spatial resolution of approximately 1.1 km x 0.9 km and provides daily, optimally interpolated, satellite-based estimates of the foundation SST (i.e., the temperature free, or nearly free, of any diurnal cycle), covering the period from January 1st, 1982, to the present. However, a major limitation of this product is that the interpolation process, especially in the presence of cloud coverage, can lead to unreliable data.
To address this issue, the L3 product (Buongiorno Nardelli et al.

2013]) was examined instead. It contains daily merged multi-sensor maps of foundation SST over the Mediterranean Sea at high (6.9km x 5.5km) and Ultra High (1.1km x 0.9km) spatial resolution. Both L4 and L3 products were downloaded from the Copernicus Marine Service Catalogue.
A comparison between L4 and L3 products revealed that cloud coverage significantly affects several days in the L4 product, compromising data quality. For this reason, the analysis primarily focused on the L3 product, selecting days with a strong SST signal for more accurate comparisons.
Regarding the SST analysis, for each map (i.e. each day) the spatial daily mean was computed and subsequently removed from the SST data originally provided by the L3 product, obtaining the SST anomaly (SSTa) as follows:

$$SSTa = SST - SST_{spatial\ mean}$$

An example of the resulting anomalies is shown in figure 2.3.1.

2.4 Ocean color

Ocean color is the perceived hue of water, produced by backscattered sunlight after interaction with the water and its microscopic constituents. These constituents typically include phytoplankton, mineral particles, and dissolved organic matter. In this study, ocean color data, like SST, are primarily used for qualitative assessments. For the analysis of ocean color, the mass concentration of chlorophyll-a (CHL-a) in seawater was considered. This product is characterized by daily temporal resolution and 1 km spatial resolution (downloaded from Copernicus Marine Service Catalogue). These data, as the SST data,

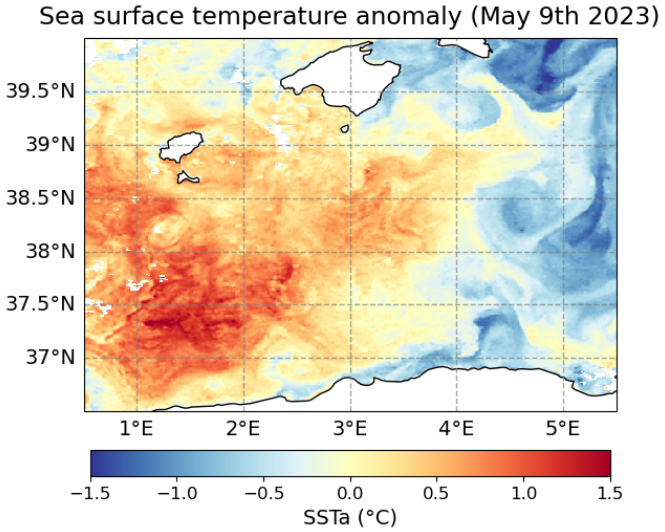

Figure 2.3.1: SSTa map of the Algerian Basin (May 9th 2023).

can depend too on the presence of clouds, resulting in a limited number of days with a distinct signal. Nevertheless, a few clear ocean color images were available during the period of May-June 2023, providing useful insights into the shape of eddy structures. An example of CHL-a concentration map is shown in figure 2.4.1.

2.5 Mediterranean forecasting system

The Mediterranean Forecasting System is an operational oceanographic forecasting system that provides analyses, reanalyses, and short-term forecasts for the entire Mediterranean Sea. Established in the late 1990s, it has been an integral part of the Copernicus Marine Service since 2015. The system operates 24/7, year-round, delivering oceanographic predictions crucial for scientific research, environmental monitoring, and marine applications. MFS is based on a coupled hydrodynamic-wave

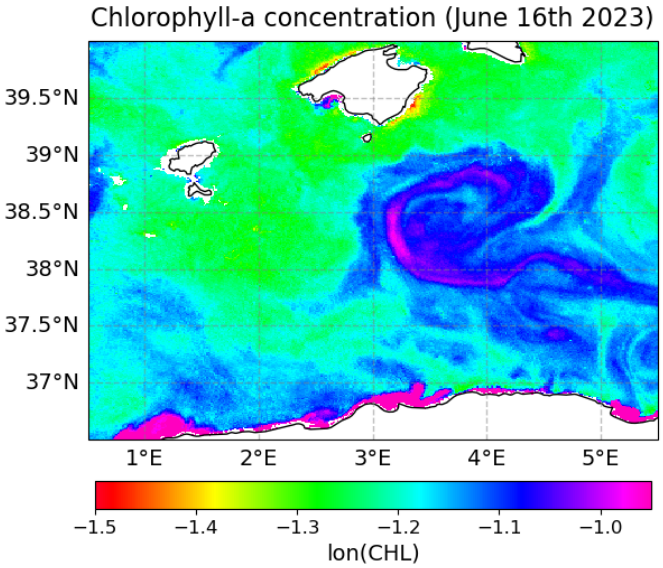

Figure 2.4.1: CHL-a concentration map of the Algerian Basin (June 16th 2023).

numerical model with data assimilation components. The hydrodynamic component relies on the NEMO (Nucleus for European Modelling of the Ocean) model, while the wave component is simulated using the WaveWatch-III model. Ocean measurements from satellites (SLA) and in situ (temperature and salinity from ARGO floats, CTD, and XBT) are assimilated on a daily basis, following a weekly cycle of assimilation. The MFS data products are accessible through the Copernicus Marine Service, including the "Mediterranean Sea Physics Analysis and Forecast" dataset, used for this work, which provides key physical oceanographic variables such as potential seawater temperature, salinity, SSH, and ocean current velocities. This dataset has a spatial resolution of 0.042° (ca. 4.7 km) with 141 vertical levels, making it a valuable resource for studying ocean circulation and mesoscale dynamics in the Mediterranean

(Clementi et al. [2018]). An example of a SLA map from the model data is given in figure 2.5.1.

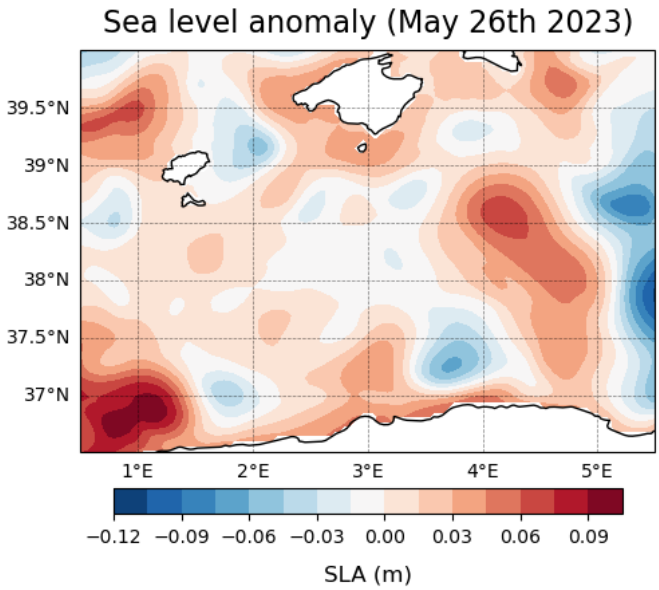

Figure 2.5.1: SLA map of the Algerian Basin from MFS model data (May 26th 2023).

Chapter 3

Comparison between SWOT and conventional altimetry

3.1 Qualitative comparison

To compare the performance of SWOT against conventional altimetry, we identified two anticyclonic eddies, referred to as eddy 1 and eddy 2, based on SLA maps from conventional altimetry (fig. 3.1.1) and MFS model data (fig. 3.1.2). These structures were further analyzed using SST and CHL-a concentration data, to provide a broader perspective on their characteristics and detectability across different observational methods.
Both eddies appear as anticyclonic structures in conventional altimetry and MFS model SLA maps. The SST anomaly field (fig. 3.1.3) reveals that eddy 1 is not clearly visible on May 26th, possibly due to increasing sea temperatures that may be hiding the signal. However, by June 1st, its signature becomes more evident. In contrast, eddy 2 is distinctly observed on June 16th, displaying a well-defined warm core. Ocean color data further corroborate the presence of these eddies (fig. 3.1.4). On June 1st, eddy 1 exhibits a clear structure, and on June 16th, eddy 2

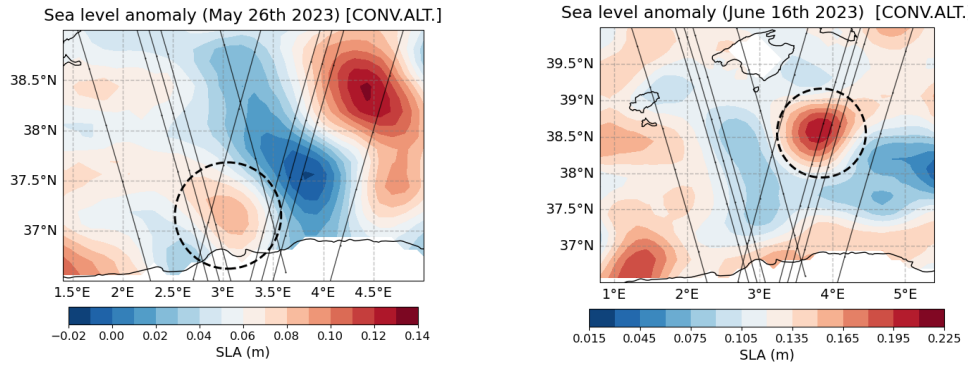

Figure 3.1.1: Sea Level Anomaly from conventional altimetry L4 product on the 26th of May, showing eddy 1 and on the 16th of June, showing eddy 2. SWOT coverage in shown in grey.

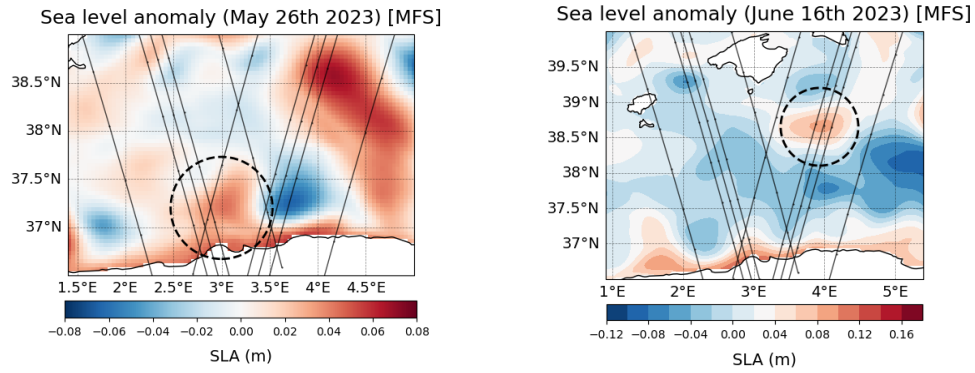

Figure 3.1.2: Sea Level Anomaly from model MFS data on the 26th of May, showing eddy 1 and on the 16th of June, showing eddy 2. SWOT coverage is shown in grey.

appears as a well-defined feature.

After identifying two anticyclonic eddy structures, we proceeded with a comparative analysis between SWOT and conventional altimetry data. This comparison aimed to assess the differences between conventional altimetry and SWOT in resolving mesoscale structures. Both datasets were evaluated against independent datasets, SSTa and CHL-a maps, to determine which

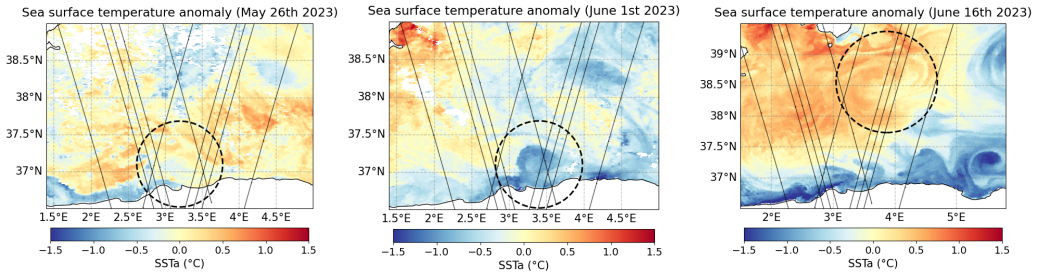

Figure 3.1.3: SST anomaly maps on the 26th of May and on the 1st of June, highlighting eddy 1, and on the 16th of June, highlighting eddy 2. SWOT coverage is shown in grey.

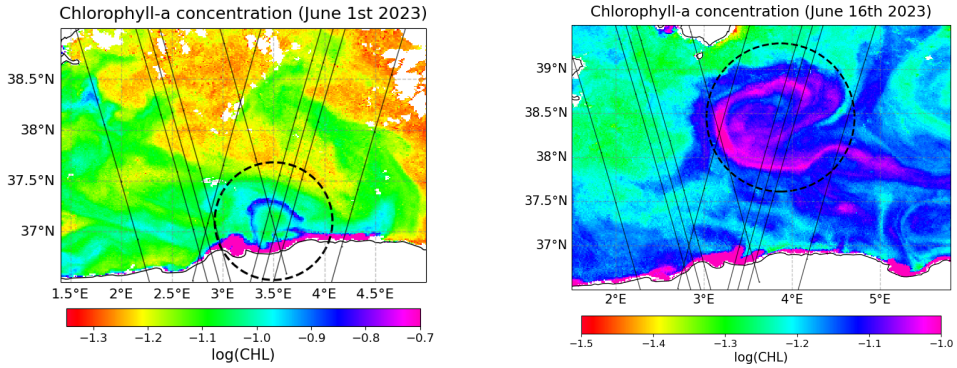

Figure 3.1.4: Chloropyll-a concentration maps on the 1st of June, highlighting eddy 1, and on the 16th of June, highlighting eddy 2. SWOT coverage is shown in grey.

provides better qualitative agreement with observed oceanographic features. Figures 3.1.5, 3.1.6, 3.1.7 and 3.1.8 illustrate how the SLA contours derived from SWOT more accurately align with features identified in SSTa and CHL-a maps, compared to the SLA contours obtained from conventional altimetry. For instance, this alignment is particularly evident on the 1st of June for eddy 1 and on the 16th of June for eddy 2, where SWOT data exhibit a stronger spatial agreement with temperature anomaly and chlorophyll maps. One of the most

evident differences is the level of detail captured by each dataset. While SWOT data resolve sharper eddy boundaries and finer-scale structures, conventional altimetry, due to its lower spatial resolution, tends to smooth out smaller features, leading to a less detailed representation of mesoscale variability. Near the coast, SWOT demonstrates a significantly higher performance than conventional altimetry in capturing features observed in SSTa and CHL-a maps. Conventional altimetry often struggles in nearshore regions due to land contamination in the altimeter signal and lower data availability, whereas SWOT's improved resolution allows for better identification of mesoscale structures interacting with coastal processes. The qualitative consistency between SLA, SSTa, and CHL-a maps indicates that SWOT effectively captures mesoscale variability, offering a more detailed representation than conventional altimetry.

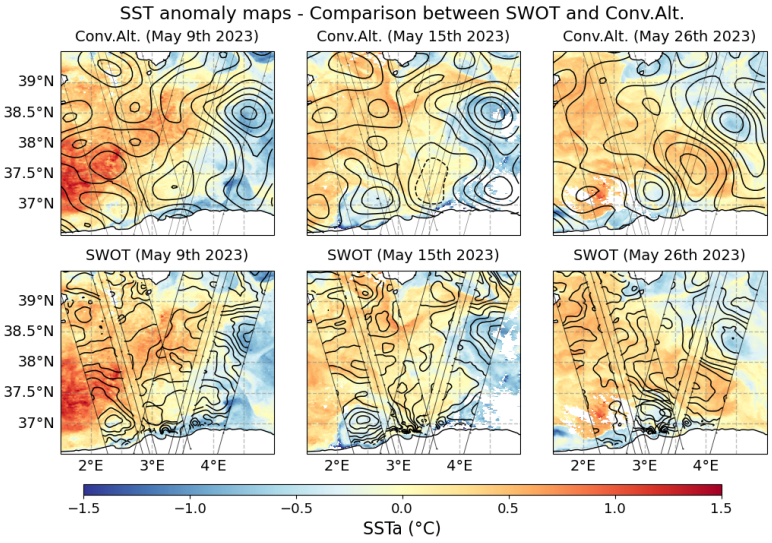

Figure 3.1.5: SSTa maps with the comparison between conventional altimetry (top) and SWOT (bottom) SLA contours, on the 9th, 15th and 27th of May.

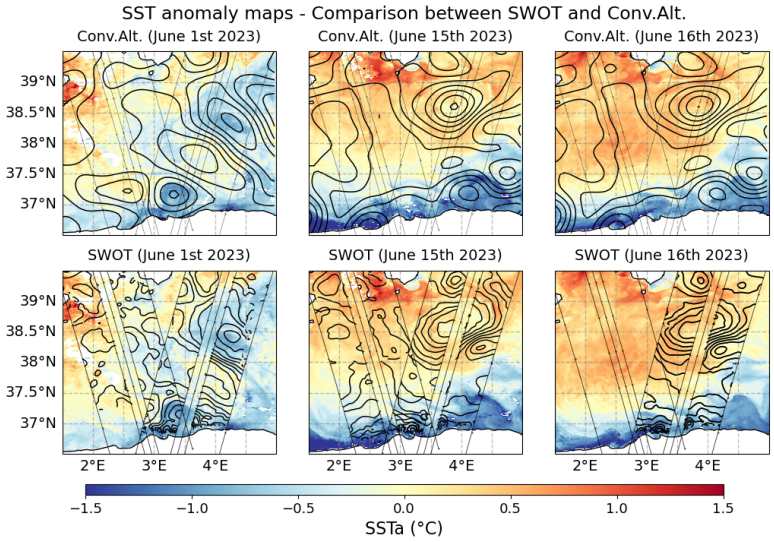

Figure 3.1.6: SSTa maps with the comparison between conventional altimetry (top) and SWOT (bottom) SLA contours, on the 1st, 15th and 16th of June.

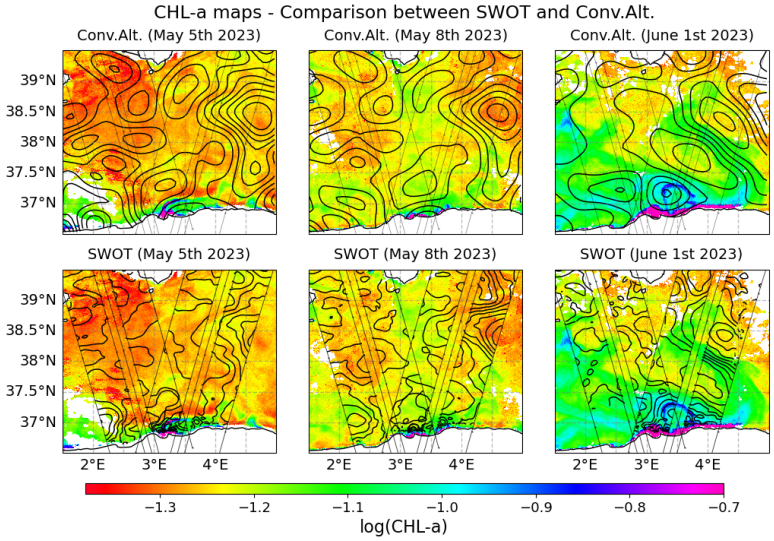

Figure 3.1.7: CHL-a maps with the comparison between conventional altimetry (top) and SWOT (bottom) SLA contours, on the 4th and 9th of May and on the 1st of June.

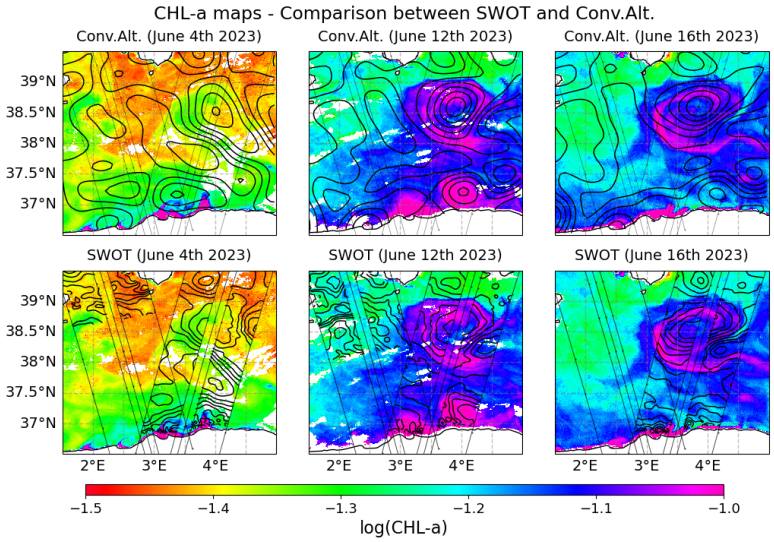

Figure 3.1.8: CHL-a maps with the comparison between conventional altimetry (top) and SWOT (bottom) SLA contours, on the 4th, 12th and 16th of June.

3.2 Statistical validation of SWOT's small scales

The SWOT mission provides a significant enhancement in resolving small-scale ocean features compared to conventional altimetry.
To quantitatively validate this improvement, a statistical approach is used to compare its variability against conventional altimetry. The method relies on analyzing the spatial standard deviation (STD) of sea surface height at different spatial resolutions. The fundamental idea is that, if SWOT effectively captures finer-scale ocean variability, its STD should decrease more rapidly than that of conventional altimetry when progressively coarsened.
The analysis follows these steps:

- To ensure a fair comparison, SWOT data is first mapped

onto a regular 1 km grid. Conventional altimetry data is then interpolated onto the same grid to match the spatial sampling.

- The spatial STD of SSH is computed at 1 km resolution, where SWOT is expected to exhibit higher variability due to its enhanced resolving capacity.
- The SSH fields are systematically smoothed by averaging the data over increasingly coarser grids (e.g. 2×2, 4×4 km up to 100×100 km). After each smoothing step, the STD is recomputed, providing a measure of how each dataset loses variability as resolution decreases. An example of the effect of coarsening on SSH fields is shown in figures 3.2.1 and 3.2.2 as the coarsening factor increases, small-scale variability is progressively smoothed out, highlighting the loss of fine-scale information.
- The STD values are then normalized relative to their initial state to quantify how rapidly each dataset loses small-scale variability.

If SWOT effectively resolves finer-scale features, its normalized STD should decay more steeply when progressively smoothed, as it initially contains more small-scale variability. In contrast, conventional altimetry, which is already limited in resolving small-scale features, should exhibit a more gradual decay.
The results confirm that SWOT retains significantly more small-scale variability at high resolution and loses it more rapidly as the resolution is coarsened (fig. 3.2.3). This behavior validates its superior resolving power for small-scale ocean features, distinguishing physical signals from noise. The difference in STD

reduction between SWOT and conventional altimetry highlights the added value of SWOT in capturing mesoscale and submesoscale structures, particularly in dynamic regions such as the Algerian Basin. In addition, it is worth noting that for SWOT, the standard deviation decreases by 5% when the resolution is coarsened from 1 km to 25 km, and by a total of 12% up to 50 km resolution. This aligns with the predicted effective resolution of SWOT (15–30 km). Similarly, for conventional altimetry, the STD curve follows the expected trend based on its effective resolution (50–70 km). The STD decreases by 5% up to a resolution of 50 km and experiences an additional 5% reduction only between 50 and 75 km resolutions.

An important consideration in this validation is that SWOT should ideally exhibit much greater variability at small scales compared to conventional altimetry. However, the extent to which this is observed depends on the methodology used. One possible explanation is that SWOT operates over a smaller available area compared to conventional altimetry, which could influence the computed statistics. In this study, SWOT available area is limited to its passes, while for conventional altimetry, the entire Western Mediterranean is considered. Nevertheless, the results indicate that SWOT effectively captures finer-scale ocean variability that conventional altimetry cannot resolve.

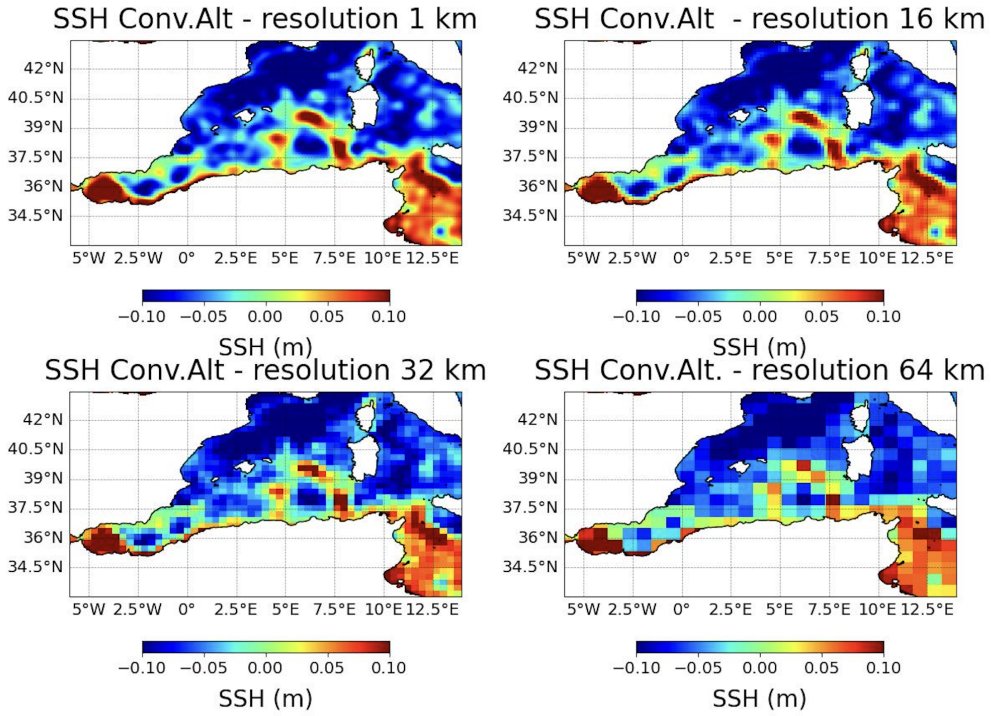

Figure 3.2.1: Effect of spatial coarsening on SSH fields from conventional altimetry. The panels show SSH maps at 1 km resolution (top left), and after applying coarsening factors of 16 (top right), 32 (bottom left), and 64 (bottom right).

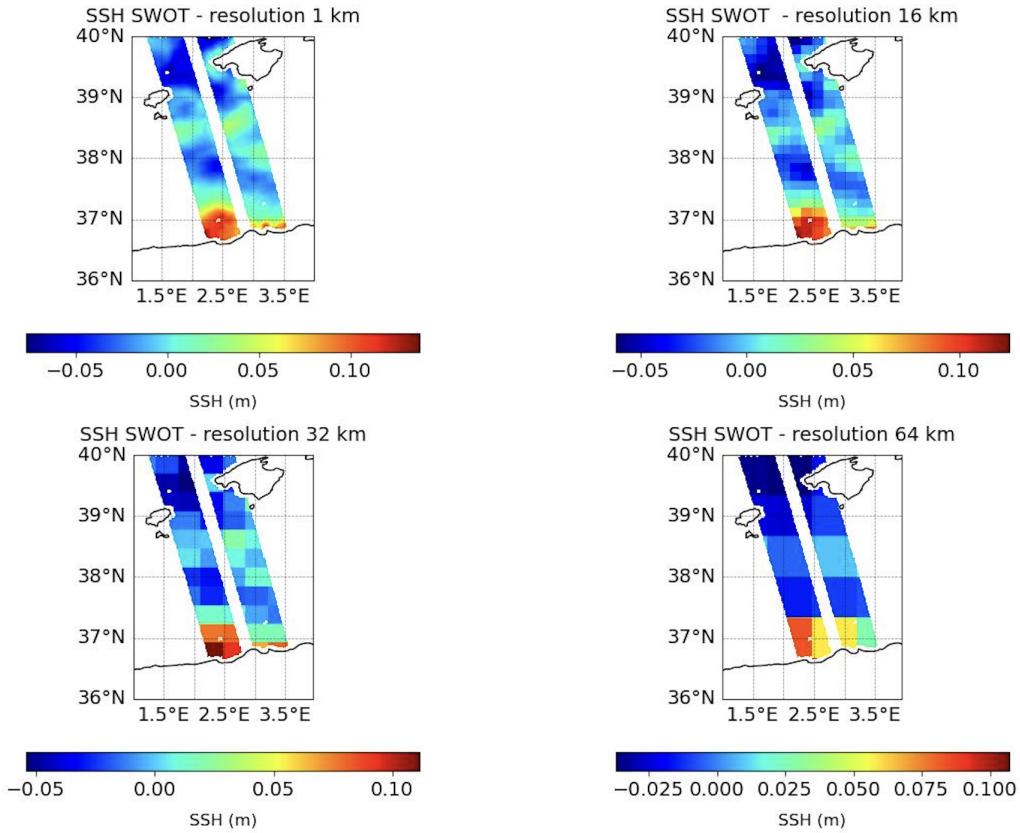

Figure 3.2.2: Effect of spatial coarsening on SSH fields from SWOT altimetry. The panels show SSH maps at 1 km resolution (top left), and after applying coarsening factors of 16 (top right), 32 (bottom left), and 64 (bottom right).

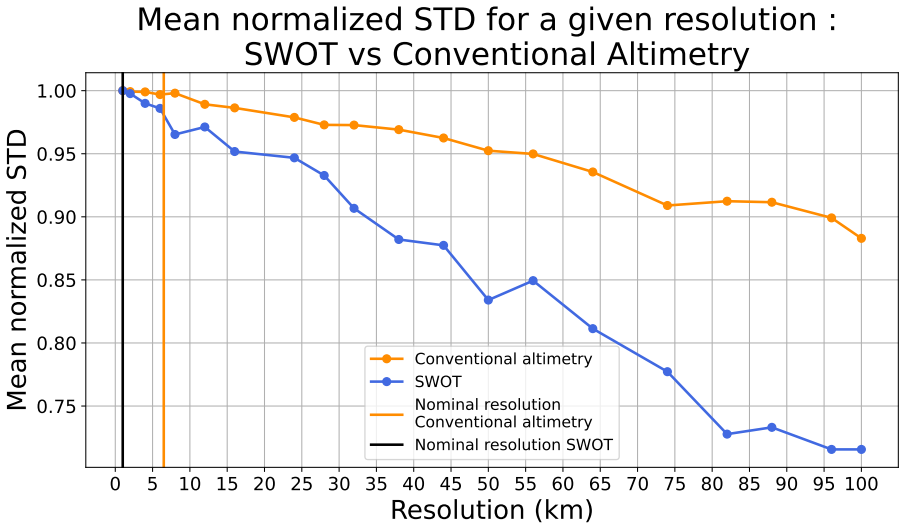

Figure 3.2.3: Normalized spatial STD of SSH as a function of the coarsening factor for SWOT and conventional altimetry.

Chapter 4

Case study of Eddy 1

4.1 Identification and observations across datasets

Eddy 1 (fig. 3.1.1, 3.1.2) was initially identified with different datasets and subsequently tracked within SWOT coverage area. Its presence was detected from the beginning of May until mid-June 202. Each dataset presented specific characteristics and limitations in observing this feature.

4.1.1 Observation with conventional altimetry

The L4 gridded altimetry product provided continuous coverage, ensuring that eddy 1 could be tracked throughout the study period. It is clearly visible on May 3rd, when eddy 1 enters SWOT coverage area and June 13th, when it exits (fig. 4.1.1). However, a noticeable deformation of the eddy's shape was observed between the 2nd and the 8th of June (fig. 4.1.2).

4.1.2 Simulation with the MFS model

The MFS model captures the eddy from its initial stages (fig. 4.1.3) until the end of May, after which it is no longer represented in

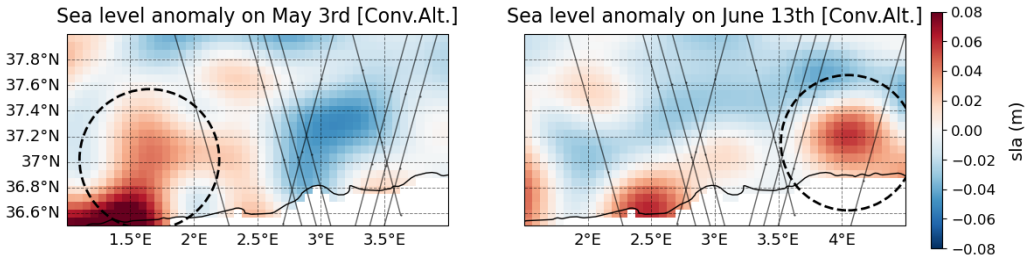

Figure 4.1.1: SLA maps of conventional altimetry (L4 product) showing eddy 1 entering and exiting SWOT coverage.

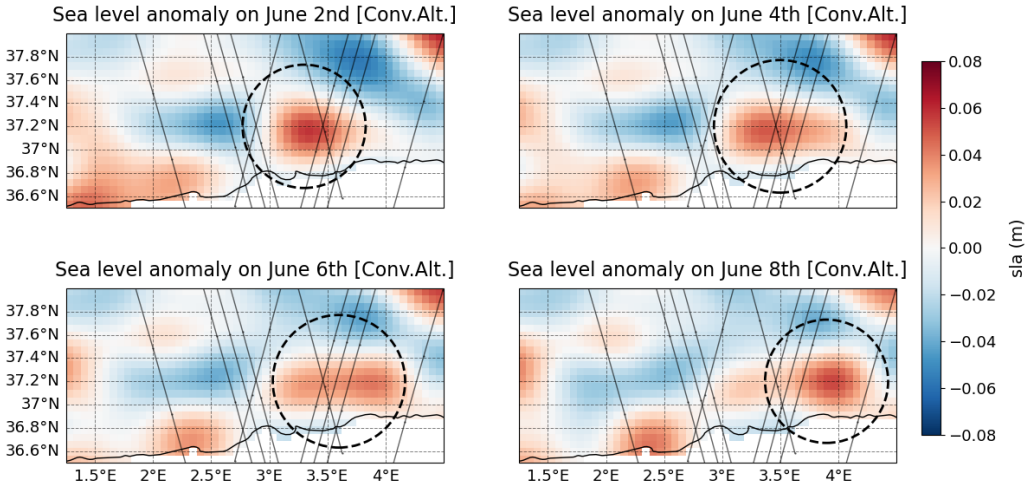

Figure 4.1.2: Deformation of eddy 1 as seen by conventional altimetry data (L4 product), between the 2nd and the 8th of June.

the simulations. Rather than being solely a limitation of the model, this disappearance (fig. 4.1.4) might reflect the actual dissipation of the original eddy.

4.1.3 Observation with SWOT

SWOT data offer a high-resolution depiction of the eddy, revealing sharper spatial features compared to conventional altimetry. Figure 4.1.5 shows eddy 1 entering and exiting SWOT coverage.

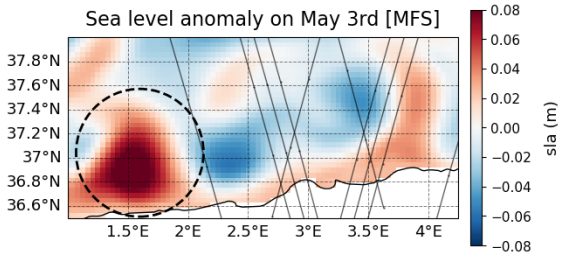

Figure 4.1.3: SLA maps of model data, showing eddy 1 entering SWOT coverage.

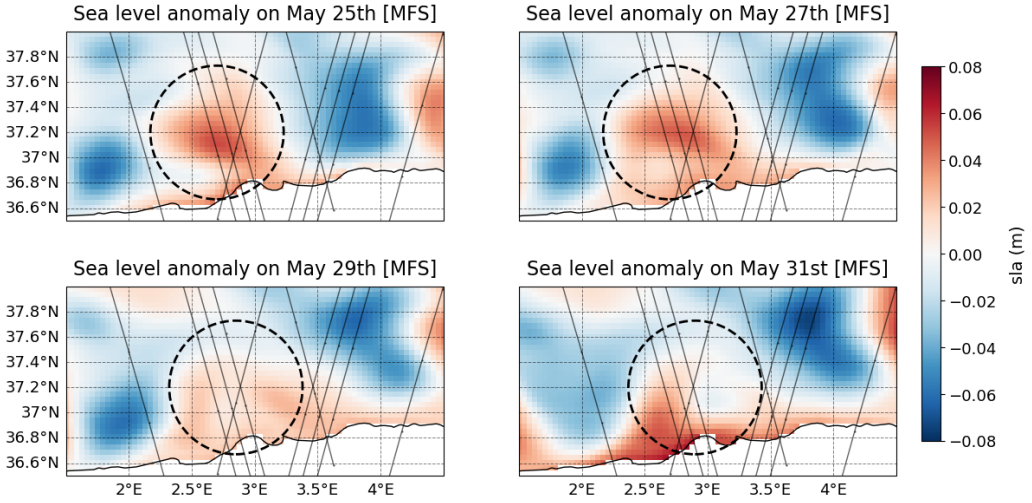

Figure 4.1.4: Dissipation of eddy 1 as predicted by the model data, during the last week of May.

However, SWOT observations are characterized by data gaps (e.g. May 7th, May 20th–22nd, May 28th) and occasional days with weaker SLA or increased noise (e.g. May 25th, May 29th). Nevertheless, the evolution of the eddy can still be monitored consistently. SWOT data show a weakening in the eddy's intensity during the final week of May (fig. 4.1.6), although this decrease is not as significant as the one predicted by the model.

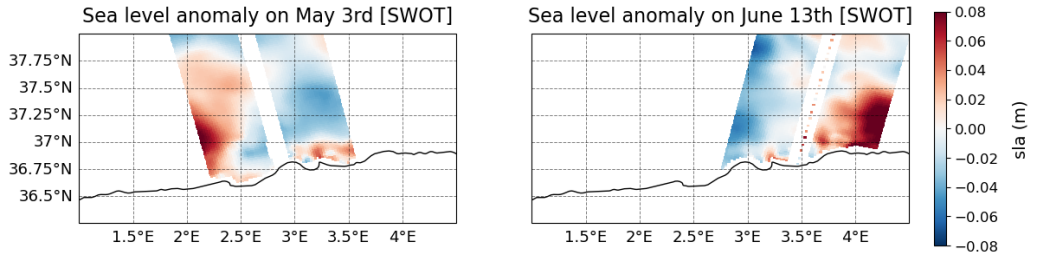

Figure 4.1.5: SLA maps of SWOT showing eddy 1 entering and exiting SWOT coverage.

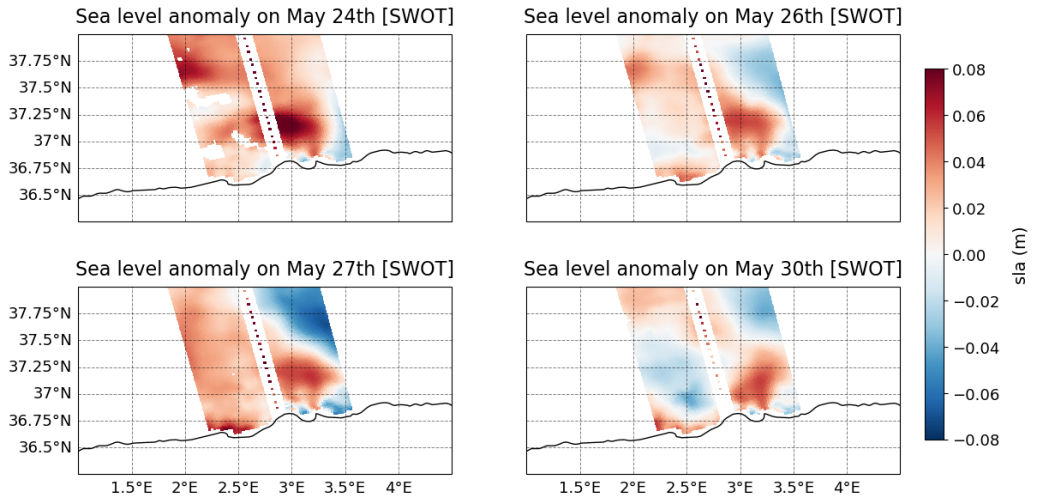

Figure 4.1.6: SLA maps of SWOT showing eddy 1 entering and exiting SWOT coverage.

4.2 Propagation and Dynamics

The propagation velocity of Eddy 1 is analyzed using three different methods and across the three datasets: conventional altimetry, MFS model and SWOT. Since automatic tracking algorithms such as PyEddyTracker (PET) cannot be directly applied to SWOT due to its discontinuous spatial coverage, alternative approaches were employed to estimate the eddy's propagation

velocity. This multi-method approach allows a robust comparison across datasets.

4.2.1 Methods

The propagation velocity of the eddy is computed using the following methods: PyEddyTracker (PET) Algorithm, SLA Max Tracking Method and Smoothed Coastline Method.

PyEddyTracker Algorithm

PET (Mason et al. [2014]) is an automated detection and tracking algorithm that identifies mesoscale eddies based on closed SLA (or ADT) contours and associated geostrophic velocity components. It subsequently tracks their displacement over time by evaluating the position of the eddy centroid. This approach is widely used for gridded altimetric and model data and provides robust estimates of eddy trajectories and velocities.
The algorithm consists of two main steps:

- Identification: Closed SLA contours are detected, with a user-defined step size between isocontours. The rotational direction of the velocity field (cyclonic or anticyclonic) is checked.
- Tracking: Once identified, eddies are tracked across successive daily fields by associating structures based on their spatial proximity, shape similarity, and overlap from one day to the next.

PET was applied to both the MFS model and the conventional altimetry datasets. SWOT data were not suitable for this ap-

proach due to their swath-based sampling and the limited number of passes over the study area.
Before detection, a high-pass Bessel filter with a cutoff wavelength of 500 km was applied to remove large-scale variability and retain mesoscale features.
The following key steps were performed for both datasets:

1. The SLA field was selected as the primary variable, along with the geostrophic velocity components.

2. A spatial subset of the study area was then extracted to focus on the eddy of interest, minimizing the influence of nearby structures in adjacent regions (fig. 4.2.1 and 4.2.2).

3. The threshold for contour detection was set to 0.001 m, based on sensitivity tests, to ensure robust eddy detection while minimizing spurious contours.

4. Eddy identification was executed on a daily basis over the study period (May 2 – June 15, 2023), with anticyclonic and cyclonic structures detected separately.

5. Tracking was subsequently performed to link identified eddies across days, constructing a continuous trajectory for the anticyclonic eddy of interest.

Following the automated detection and tracking, visual inspection of the identified eddy contours was carried out for the whole period, ensuring that the detected structure corresponded to eddy 1.
Although PET effectively captured the eddy's evolution, the algorithm failed to detect the structure on certain days. Specifically, gaps were observed in the conventional altimetry dataset

between May 2 and May 8, and between June 3 and June 7. Similarly, gaps appeared in the MFS model between May 7 and May 11. However, the number of successful identifications was sufficient to estimate the propagation velocity. The days with successful detections will be later used as a reference for calculating velocities using the two alternative methods.
Representative examples from both datasets are shown in figure 4.2.1 and 4.2.2, highlighting the capability of PET to delineate the eddy's shape and monitor its evolution over time.
As already noted in Section 4.1, this analysis revealed that the conventional altimetry dataset shows a deformation of the eddy in early June, when, in fact, the identification was not possible, while the MFS model shows the eddy weakening and dissipating by the end of May, when PET algorithm stopped being able to recognize the eddy.

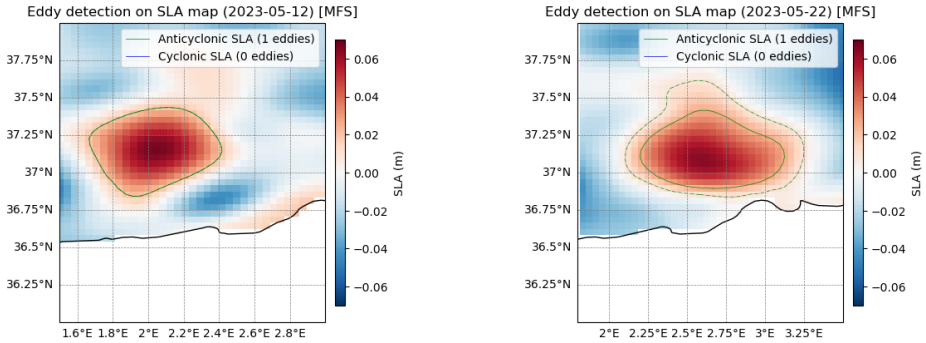

Figure 4.2.1: Eddy detection performed on MFS model SLA maps by PET algorithm on may 12th and 22nd.

SLA Max Tracking Method

The SLA maximum method is based on the identification of the point of maximum SLA within the eddy structure and tracking

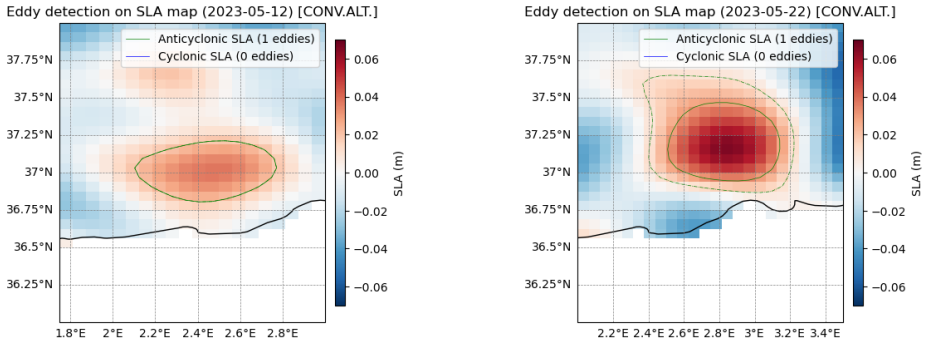

Figure 4.2.2: Eddy detection performed on conventional altimetry SLA maps by PET algorithm on May 12th and 22nd.

its displacement over time. The reference days selected for the calculation were those on which the PET algorithm successfully performed eddy detection.
The steps for applying this method were as follows:

1. The point of maximum positive SLA within the anticyclonic structure was selected, restricting the search to the area surrounding the eddy to avoid selecting spurious maxima unrelated to the feature of interest.

2. This position was recorded for each day identified by PET algorithm.

3. The displacement of the SLA maximum between consecutive days was calculated to estimate the propagation velocity.

This approach was applied to all three datasets. However, special care was required when considering SWOT data. On days when the eddy was either entering or exiting the SWOT coverage, or switching between passes, the detected maximum SLA could be misleading. In these cases, the observed maximum may

not correspond to the actual SLA peak, as it could lay outside the swath. This limitation was acknowledged and considered in the interpretation of the results.

Smoothed Coastline Method

This method estimates the eddy's displacement relative to a smoothed coastline, obtained with a 60 km moving average. The smoothed coastline is shown in figure 4.2.3.

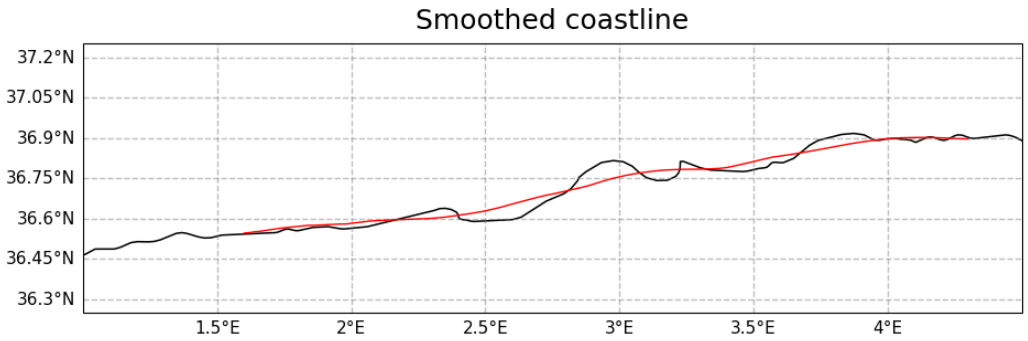

Figure 4.2.3: Smoothed coastline obtained with a 60 km moving average.

The intersection point between the eddy contour and the smoothed coastline was used as a reference position. In addition to the smoothing process, an offset is applied to adjust the coastline position, ensuring that it intersects specific points of the eddy contour, according to the following criteria:

- Before early June: the easternmost intersection point is used.
- After early June: the westernmost intersection point is considered. This shift is due to the fact that, with SWOT data, in the second part of the propagation, the easternmost in-

tersection lays outside the swaths. An example can be seen in figure 4.2.4.

- The reference point is always chosen under the condition that it intersects both contours.

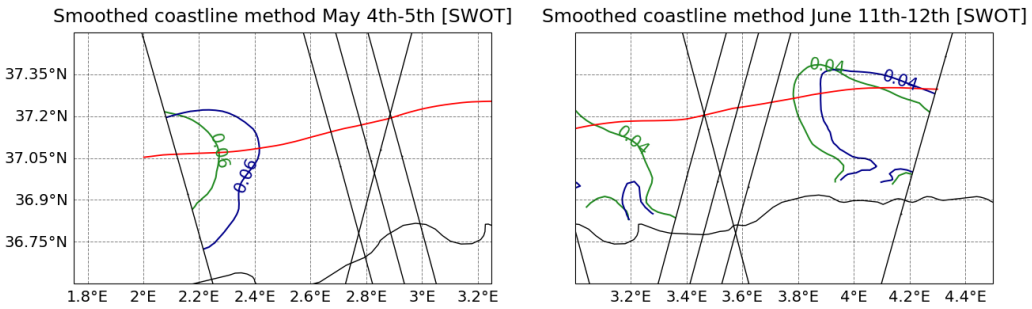

Figure 4.2.4: Examples of the smoothed coastline method applied to SWOT data. The smoothed coastline is depicted in red. The green and the blue contours represent the two consecutive days considered.

As in the SLA max tracking method, the reference days selected for the calculation were those with successful detection performed by PET algorithm.
This method is also applied to all three datasets with specific considerations for each:

- SWOT: The 6 cm contour was used until May 24, after which the 4 cm contour was selected to account for the weakening of the eddy, as previously mentioned.
- Conventional Altimetry: The 3 cm contour was consistently used.
- MFS Model: The 5 cm contour was adopted initially, but towards the end of May, the eddy progressively weakened and the 3 cm contour was selected. From May 29 onwards,

even smaller contours were no longer present, marking the dissipation of the eddy in the model.

4.2.2 Results

The propagation velocity time series derived are presented in figures 4.2.5, 4.2.6, and 4.2.7, organized by dataset for conventional altimetry, MFS model data, and SWOT, respectively. Additionally, figures 4.2.8, 4.2.9, and 4.2.10 present the results organized by method, showing the PET algorithm, the Smoothed Coastline method, and the SLA max tracking method.

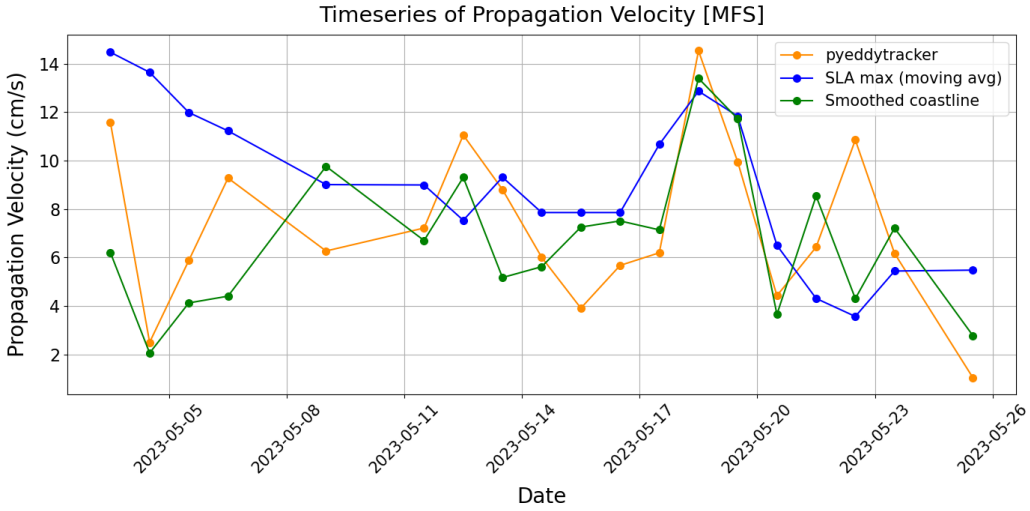

Figure 4.2.5: Propagation velocity of Eddy 1 based on MFS model data, with three methods: PET algorithm (orange), SLA max tracking (blue) and smoothed coastline method (green).

Among the three methods, the Smoothed Coastline method shows the best agreement with the PET algorithm in both the MFS model and conventional altimetry datasets, indicating that it provides a reliable estimate of propagation velocity. In contrast, the SLA max tracking method exhibits more variability

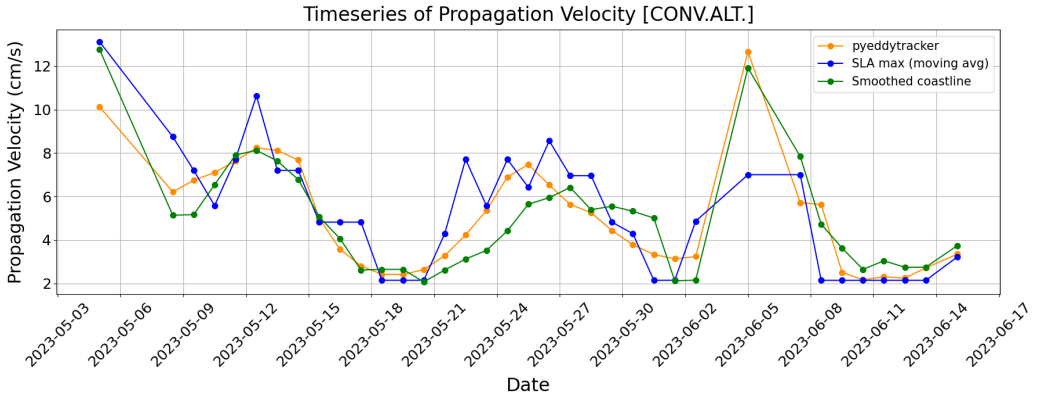

Figure 4.2.6: Propagation velocity of Eddy 1 based on conventional altimetry data, with three methods: PET algorithm (orange), SLA max tracking (blue) and smoothed coastline method (green).

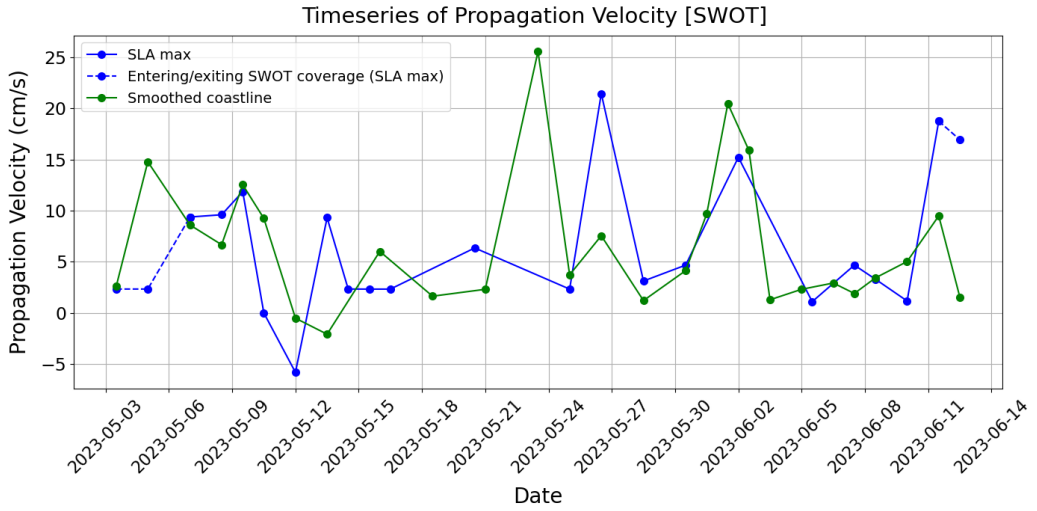

Figure 4.2.7: Propagation velocity of Eddy 1 based on SWOT data, with two methods: SLA max tracking (blue) and smoothed coastline method (green). The blue dashed line indicates maxima of SLA on days corresponding to the eddy entering or exiting SWOT coverange, hence unreliable.

and oscillations. To mitigate these fluctuations, a 3-point running mean was applied to obtain a smoother time series.
Notable discrepancies emerge in specific periods, reflecting both

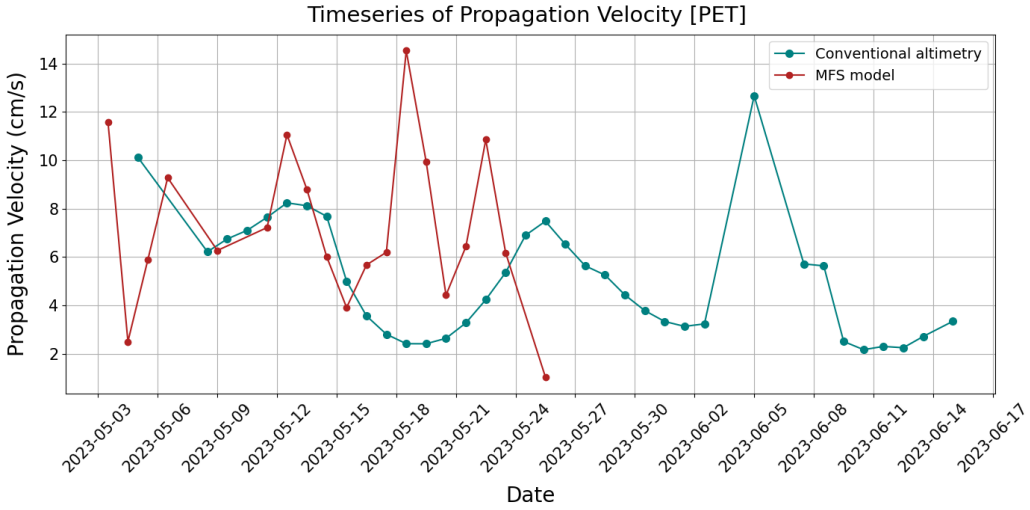

Figure 4.2.8: Propagation velocity of Eddy 1 with PET algorithm, applied to conventional altimetry (light blue) and MFS model (red) data.

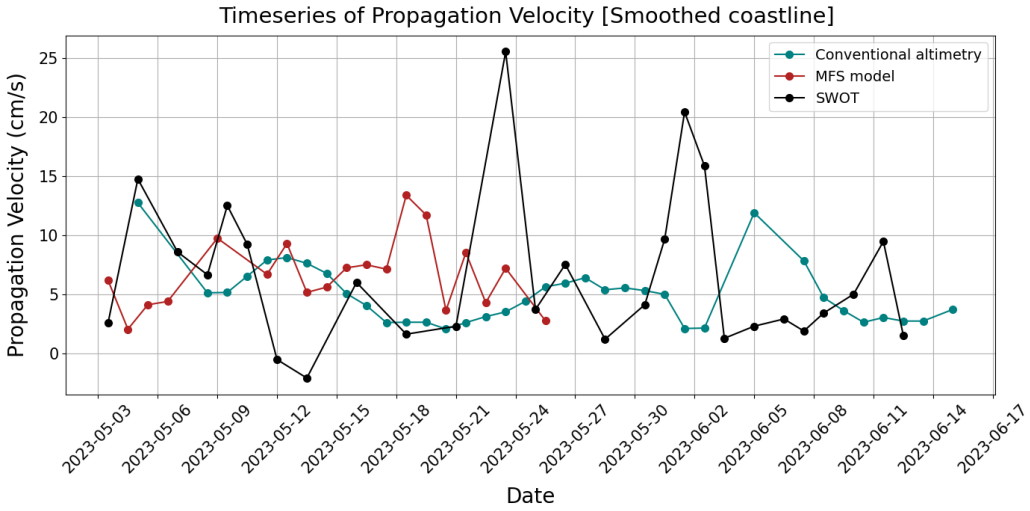

Figure 4.2.9: Propagation velocity of Eddy 1 with the Smoothed Coastline method, applied to conventional altimetry (light blue), MFS model (red) and SWOT (black) data.

methodological limitations and the evolution of eddy 1 itself. A clear example is the sharp acceleration signal detected in the

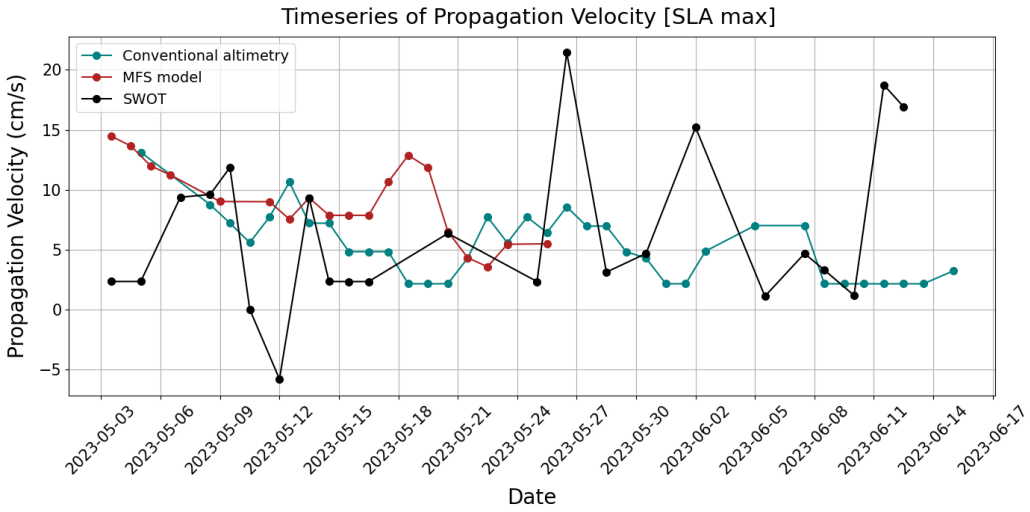

Figure 4.2.10: Propagation velocity of Eddy 1 with the SLa max tracking method, applied to conventional altimetry (light blue), MFS model (red) and SWOT (black) data.

SWOT-derived velocity on May 23-24 with the smoothed coastline method and on May 26-27, with SLA max tracking method. A similar acceleration signal can be noticed in the velocity derived from MFS model data with PET algorithm. This anomaly is likely associated with the weakening of the eddy's intensity, already observed with both SWOT and model datasets.
From early June onwards, a few more issues arise. The MFS model fails to track the eddy beyond the end of May, suggesting that it dissipates within the simulation. Conventional altimetry, on the other hand, shows a deformation of the eddy structure (fig. 4.1.2), coinciding with a period where no along-track altimetric data is available. Figure 4.2.11 shows along-track data during the period coinciding with the deformation. It is clear that on the area affected by the deformation (3-4°E, 36.8-37.5°N) no along-track data is available. This suggests that the observed

SLA patterns in this phase are heavily dependent on interpolation, reducing the reliability of velocity estimates. SWOT data, on the other hand, still exhibit an eddy-like structure during this period. However, following the initial decline in intensity observed in late May, the eddy experiences a deformation and a new intensification (fig. 4.2.12).

These findings collectively indicate that the deformation of eddy 1, as depicted by conventional altimetry (fig. 4.1.2), may not be reliable. By incorporating SWOT and model data, a more coherent picture of the eddy's evolution emerges. Both datasets suggest a weakening of the eddy's intensity in late May. However, while the model predicts the complete dissipation of the eddy (fig. 4.2.13), SWOT continues to detect a coherent eddy structure beyond this period (fig. 4.2.12). This suggests that, rather than a direct continuation of the original eddy, the feature observed in early June by SWOT is likely a newly formed eddy, generated after the dissipation of the previous one.

These results emphasize SWOT's capability to resolve finer spatial details that conventional altimetry fails to capture. Its higher resolution and improved coverage allow for a more precise depiction of mesoscale structures, revealing features that might otherwise be neglected due to the interpolation and lower spatial resolution of conventional altimetry.

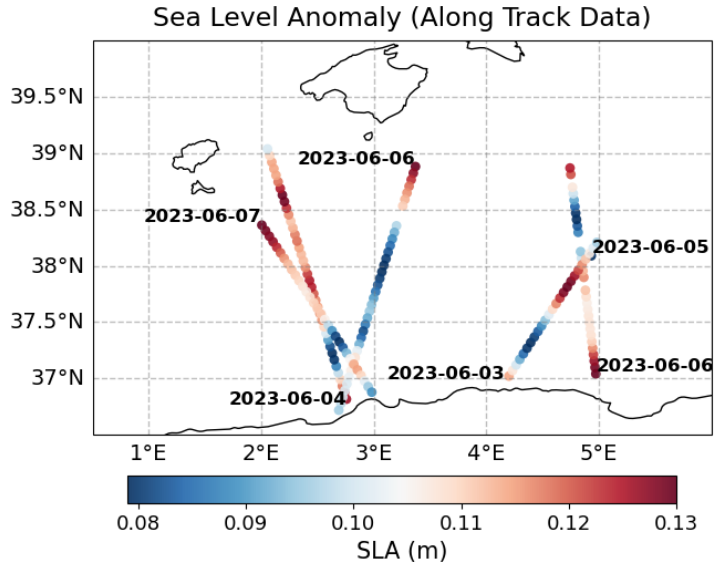

Figure 4.2.11: Satellite along-track data (L3 product) during the first week of June.

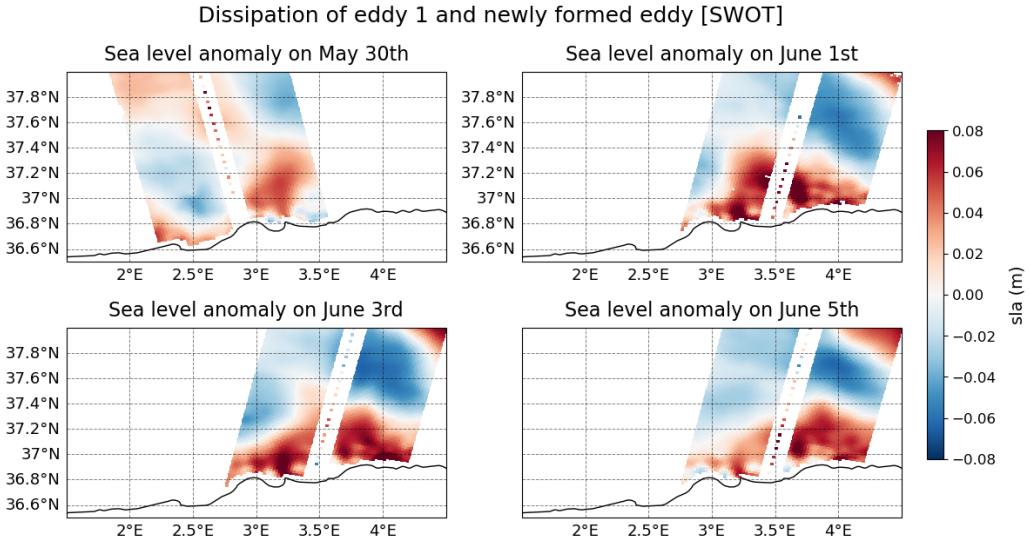

Figure 4.2.12: SLA maps of SWOT showing eddy 1 in the last phase of its life cycle (upper left) and the new structure formed (upper right and bottom).

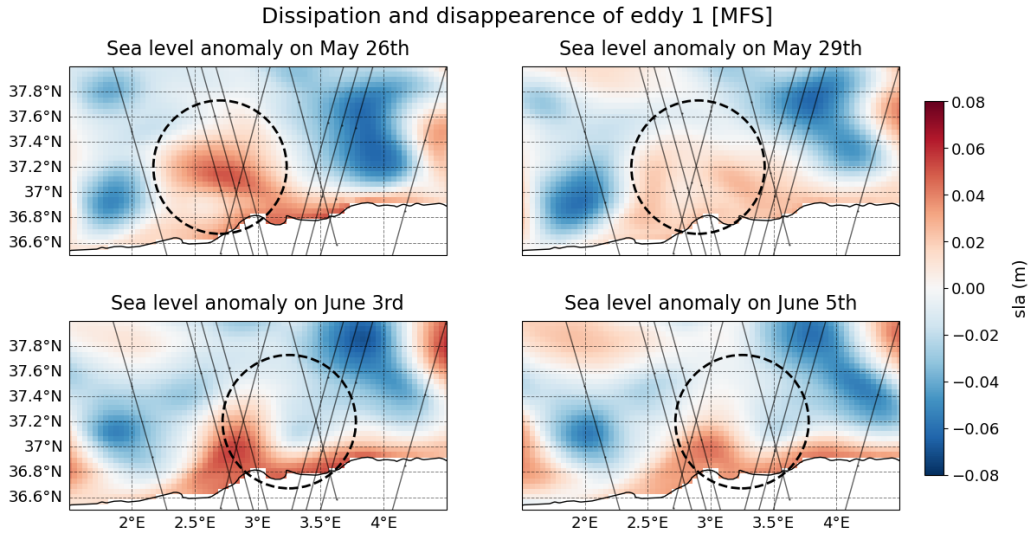

Figure 4.2.13: SLA maps of model data showing eddy 1 (upper left), eddy 1 dissipating (upper right) and its absence in early June (bottom).

4.3 Potential Vorticity and Interaction with Bathymetry

The evolution of eddy 1 suggests a weakening phase towards the end of May, ultimately leading to its dissipation. To better understand this process, we analyze its potential vorticity and vertical extent, as the three-dimensional structure of the eddy plays a key role in its stability and interaction with bathymetry. This analysis is carried out using the MFS model data.

4.3.1 Eddy depth estimation

Estimating the depth of an eddy is fundamental to understand its vertical structure and the extent of its influence on the underlying water masses. The depth can be interpreted as the level below which the flow associated with the vortex becomes negligi-

ble, marking the lower boundary of its dynamical impact. In this study, the depth of eddy 1 was estimated using the geostrophic velocity field provided by the MFS model. In particular, the approach relied on the evaluation of the decay of geostrophic velocity with depth. The estimation of the geostrophic velocities at depth was carried out using hydrostatic and geostrophic balance assumptions.
The procedure followed these steps:

1. Temperature, salinity, SSH, pressure levels, latitude, longitude and depth were extracted from the MFS model dataset.

2. Calculation of density: Using Absolute Salinity (SA) and Conservative Temperature (CT), the density ρ was computed at each grid point and depth level, applying the TEOS-10 equation of state. TEOS-10 is based on a Gibbs function formulation from which all thermodynamic properties of seawater can be derived in a thermodynamically consistent manner (`https://teos-10.org/`). An initial approximation for the pressure, in order to calculate the density, was obtained from depth and latitude.

3. Reference density: A reference density ρ_0 was defined as the horizontal average of the surface density field, in the Algerian Basin.

4. Neglecting the atmospheric pressure, the surface pressure term was computed as:

$$\mathrm{p}_{surface} = \rho_0 g \eta \tag{4.1}$$

where ρ_0 is the reference surface density, g is the gravitational acceleration and η is the sea surface height.

5. The pressure anomaly at depth was calculated using the hydrostatic balance:

$$p_{hydrostatic}(z) = g \int_{z}^{0} \delta\rho(z')dz' \tag{4.2}$$

6. Total pressure field: The total pressure field was obtained as the sum of the surface pressure contribution and the hydrostatic pressure anomaly:

$$p(z) = p_{surface}(z) + p_{hydrostatic}(z) \tag{4.3}$$

7. Horizontal pressure gradients: The horizontal gradients of pressure were computed along the zonal (x) and meridional (y) directions.

8. Geostrophic velocities: The geostrophic velocity components were derived from the pressure gradients:

$$u_g = -\frac{1}{\rho f}\frac{\partial p}{\partial y}, \quad v_g = \frac{1}{\rho f}\frac{\partial p}{\partial x} \tag{4.4}$$

9. Finally, the magnitude of the horizontal velocity was computed as:

$$\mathbf{v_g} = \sqrt{u_g^2 + v_g^2} \tag{4.5}$$

Vertical sections of geostrophic velocity were analyzed along both a zonal and a meridional section crossing the eddy (figure 4.3.1 – latitudinal section; figure 4.3.2 – longitudinal section). Additionally, an average velocity profile was computed over a box encompassing the structure (fig. 4.3.3).
The profile reveals that velocity decreases to 15% of its surface maximum (30 cm/s) at a depth of approximately 250 m, where

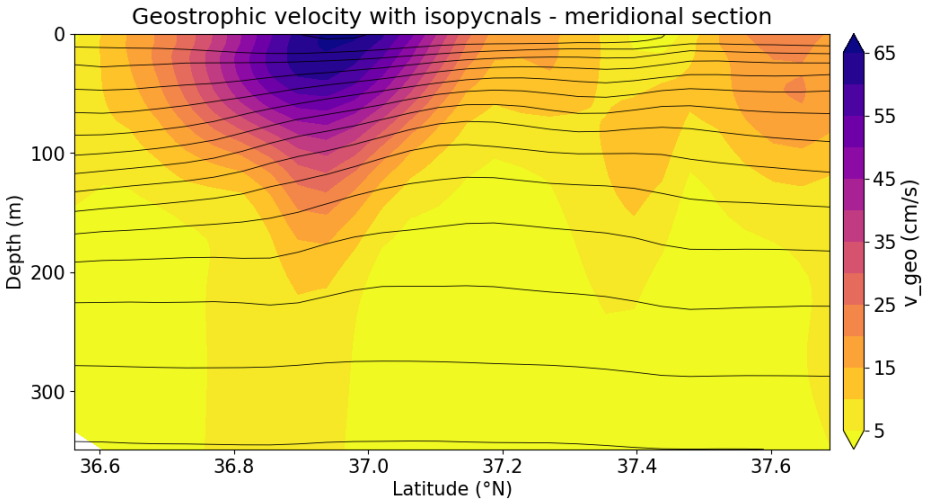

Figure 4.3.1: Geostrophic velocity (meridional section) with overlaid isopycnals.

it reaches a value smaller than 5 cm/s. This level is therefore taken as the estimate of the eddy's lower boundary.
To further validate this estimate, the density field was analyzed by overlaying isopycnals on the vertical velocity sections. The isopycnals exhibit a gradual flattening and become flat before 300 m, suggesting that the dynamical influence of the eddy weakens significantly before this depth. The consistency between the velocity-based estimate and the density structure supports the choice of 250 m as a reasonable approximation of the eddy depth. This finding is consistent with the studies conducted by Poulain et al. [2021] and Escudier [2014].

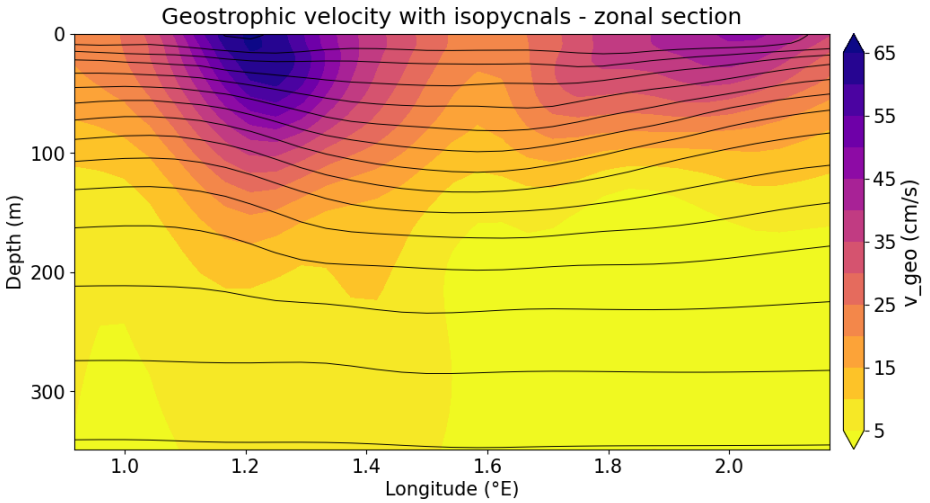

Figure 4.3.2: Geostrophic velocity (zonal section) with overlaid isopycnals.

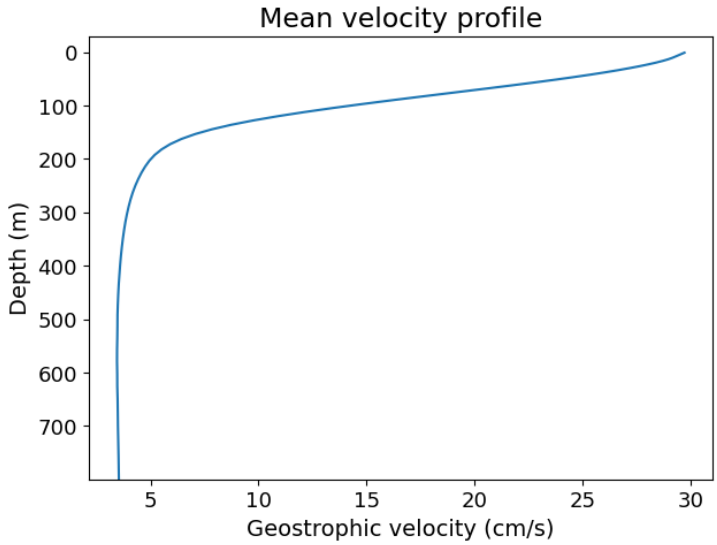

Figure 4.3.3: Mean velocity profile of eddy 1. The mean velocity is computed over a box enclosing the eddy.

4.3.2 Potential vorticity

Potential Vorticity (PV) is a fundamental conserved quantity in geophysical fluid dynamics, playing a crucial role in the understanding of mesoscale structures such as eddies and their interaction with bathymetry. It encapsulates the effects of planetary and eddy rotation, as well as variations in fluid column depth, making it a powerful diagnostic tool for investigating the evolution of oceanic vortices. Under adiabatic and inviscid conditions, PV is materially conserved following a fluid parcel, meaning that any change in PV must arise from non-conservative processes such as friction, mixing, or diabatic effects. This conservation principle makes PV particularly useful for studying eddy dynamics and their potential exchanges with surrounding waters. In this study, we adopt the shallow-water and geostrophic approximations, which describe barotropic motions. Under these assumptions, PV is expressed as:

$$PV = \frac{\zeta_R + f}{H + \eta} \tag{4.6}$$

where:

- f is the Coriolis parameter, representing planetary vorticity,
- ζ_R is the relative vorticity, defined as:

$$\zeta_R = \frac{\partial v}{\partial x} - \frac{\partial u}{\partial y} \tag{4.7}$$

  which measures the local rotation of the flow,
- H is the depth of the water column,
- η is the sea surface height.

Thus, the conservation of potential vorticity is described as:

$$\frac{D}{Dt}\left(\frac{\zeta_R + f}{H + \eta}\right) = 0 \tag{4.8}$$

This formulation highlights that changes in PV can arise from three main factors: variations in the flow's vorticity ζ_R, modifications in the water column thickness (due to bathymetric variations or sea surface anomalies), and, to a lesser extent, changes in the Coriolis parameter f. Given that eddy 1 remains within a relatively narrow latitudinal range, variations in f are expected to be minimal compared to the other terms.

The conservation of PV implies that any significant variation in the water column thickness can influence an eddy's structure and propagation. This effect becomes particularly relevant in regions characterized by strong bathymetric gradients, such as the Algerian Basin, where interactions with the seafloor can modify the eddy's dynamics. As an eddy moves over a sloping bottom, adjustments in water column thickness may lead to changes in vorticity, potentially altering its stability and trajectory.

In this study, we assess the PV distribution within eddy 1, with the goal of understanding its evolution. The analysis is based on the MFS model dataset, which provides three-dimensional oceanographic fields necessary for its computation.

Since the eddy's depth has been previously estimated at approximately 250 m, this allows us to evaluate whether its vertical extent and structure could have played a role in modulating its interaction with the bathymetry. To further investigate this, we analyze the temporal evolution of PV and its individual components over the study period.

4.3.3 Analysis of PV Components

Relative Vorticity (ζ_R)

The relative vorticity ζ_R within the eddy exhibits a clear increasing trend, particularly in the final phase leading to its dissipation (fig. 4.3.4). Given that

$$\zeta_R \sim \frac{V}{R} \tag{4.9}$$

where V is the geostrophic velocity and R is the radius of the eddy, a possible explanation lies in the observed contraction of the eddy area over time (fig. 4.3.5). Here, R is estimated by approximating the eddy to a circle, while V is computed as the mean value of the geostrophic velocity magnitude within the eddy. This value is obtained by first averaging the velocity over the water column, limited to eddy's depth (250 m) or to the local bathymetric depth when shallower, and then averaging spatially over the eddy area. As the eddy shrinks, its radius R decreases, leading to an increase in ζ_R (decrease when considered in its absolute value), if the velocity V remains relatively stable.
The velocity-to-radius ratio (V/R) confirms this trend, following the same evolution as ζ_R (fig. 4.3.6). To further investigate this hypothesis, we separately analyzed the variations in V and R during the last phase of the eddy's lifetime (fig. 4.3.7). The results indicate that while V undergoes only minor fluctuations, R shows a marked decrease.
Overall, these findings suggest that the dissipation of the eddy is accompanied by a progressive reduction in its spatial extent, with relative vorticity approaching zero as a product of this contraction. This behavior aligns with the expected dynamics of mesoscale eddies nearing the end of their life cycle, where energy is progressively dissipated, and the eddy structure collapses.

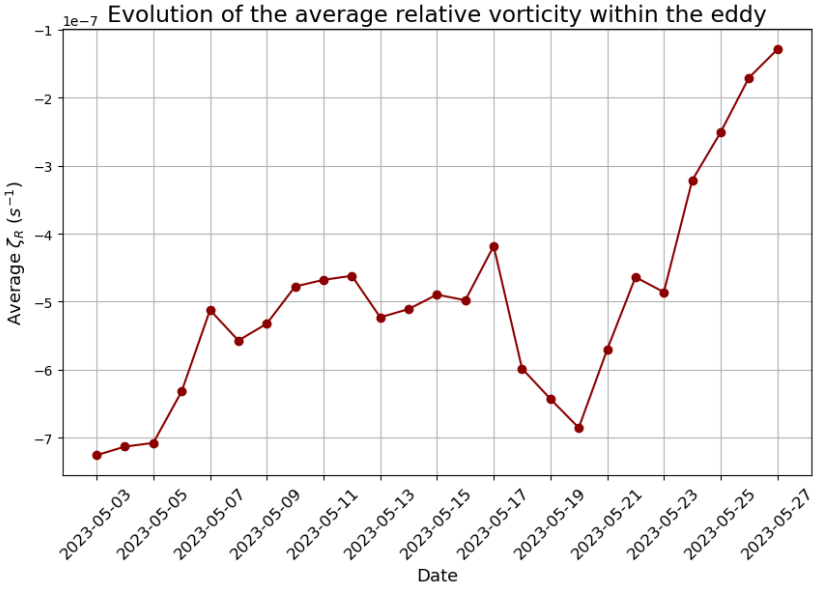

Figure 4.3.4: Evolution of the relative vorticity of eddy 1.

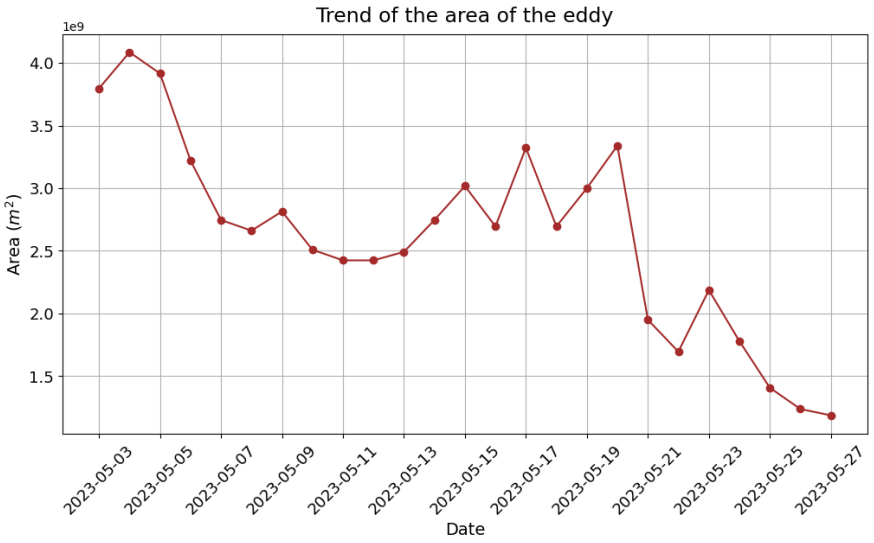

Figure 4.3.5: Evolution of the area of eddy 1.

Coriolis Parameter (f)

The Coriolis parameter f varies minimally due to the limited latitudinal displacement of the eddy (fig. 4.3.8). Consequently,

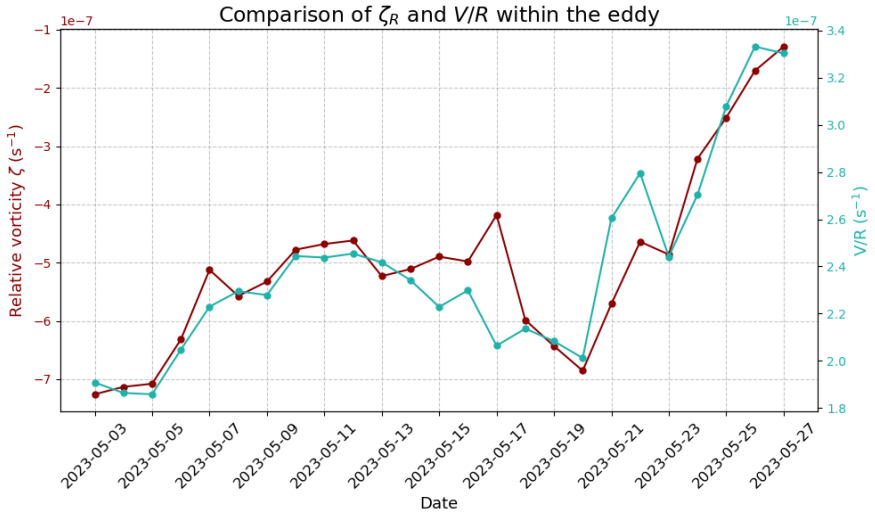

Figure 4.3.6: Comparison between the relative vorticity ζ_R of eddy 1 and V/R.

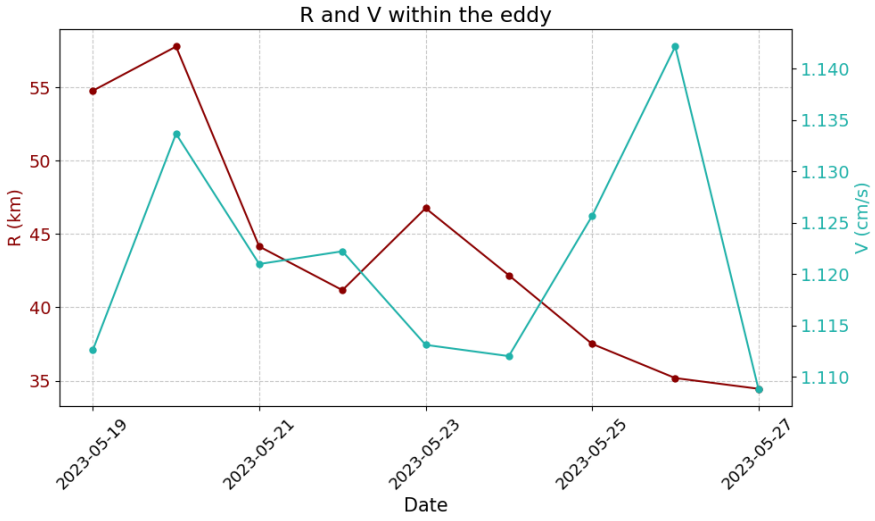

Figure 4.3.7: Variation of V and R during the last phase of eddy 1's lifetime.

its contribution to PV variations is negligible.

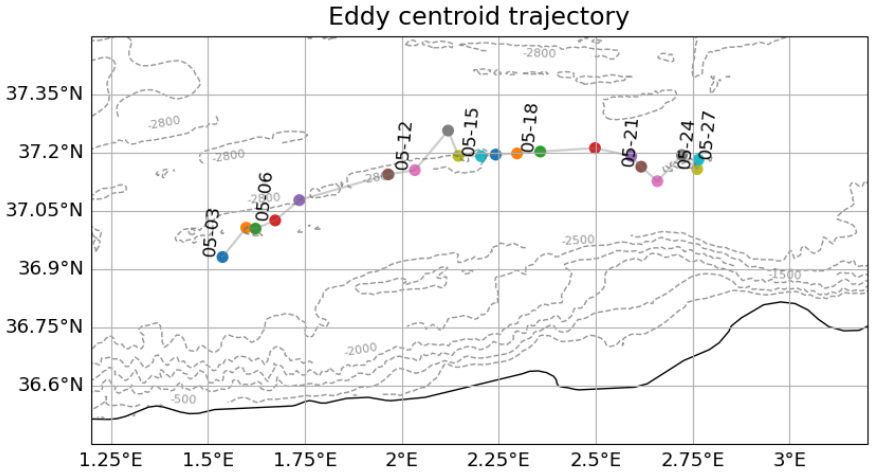

Figure 4.3.8: Trajectory of the centroid of eddy 1.

Sea Surface Height (η)

The sea surface height η shows an increasing trend. This is expected if we consider the eddy approaching shallower bathymetry. In fact, in order to keep PV conserved, if H decreases η must increase.

Depth (H)

In figure 4.3.10, the timeseries of H is presented. H is taken as the minimum value of the depth within the area of the eddy. The plot shows a decrease in H around the 11th of May and doesn't increase again until the 21st. During this period the minimum of H reaches values below the estimated eddy depth (250 m), indicating a possible interaction of eddy 1 with the bathymetry.

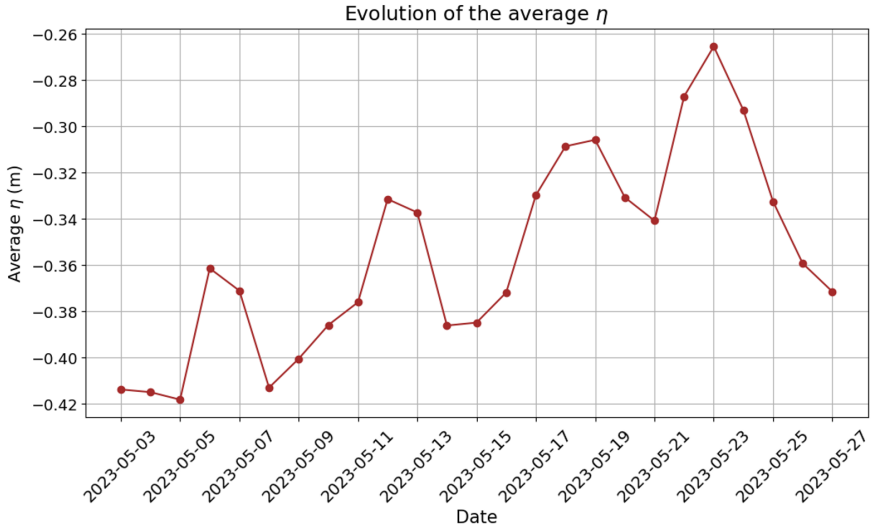

Figure 4.3.9: Evolution of the sea surface height within the eddy.

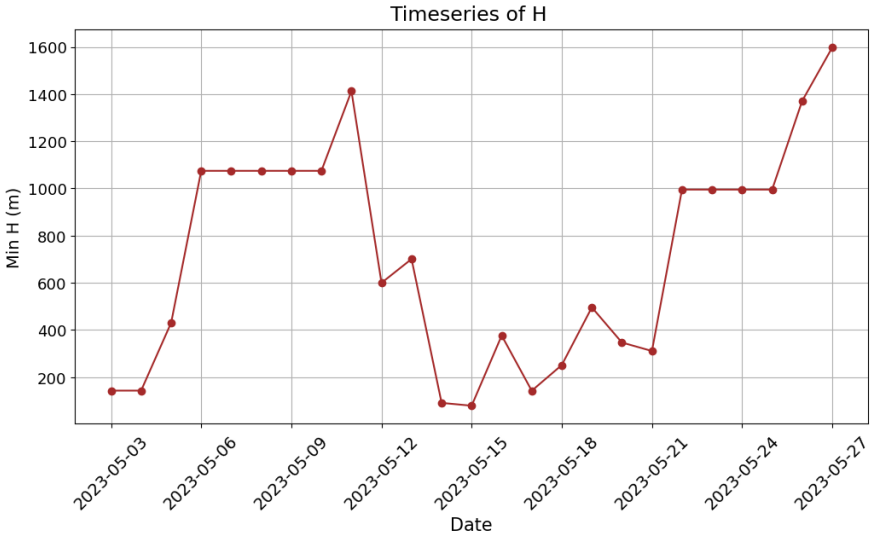

Figure 4.3.10: Timeseries of H within the eddy.

4.3.4 Testing PV Conservation

To assess whether PV is conserved, we examine its temporal evolution over the study period. If PV remains approximately

constant, this would indicate that the eddy's evolution is primarily governed by geostrophic and barotropic dynamics. However, deviations from conservation suggest the influence of additional processes such as ageostrophic motions or topographic interactions. Figure 4.3.11 shows the tendency of potential vorticity over time, calculated as the ratio of PV differences between consecutive days and Δt. Our results indicate that PV is not strictly conserved, particularly in the second stage of the eddy's lifecycle. To further explore this, we analyze the ageostrophic component of the velocity of the eddy, which provides a measure of increasing non-geostrophic contributions and could lead to the non-conservation of PV. On average, the ageostrophic component of the velocity represents around the 5% of the geostrophic component.
The ratio of ageostrophic to geostrophic velocity (4.3.12) exhibits oscillatory behavior, with notable peaks that appear to correspond with increases in PV tendency. Specifically:

- Around May 6th, both the PV tendency and the ageostrophic-to-geostrophic velocity ratio reach a local maximum, suggesting an early deviation from PV conservation.
- Between May 14th and May 16th, there is a gradual increase in both variables, indicating a progressive shift towards a more ageostrophic regime.
- A pronounced peak in the PV tendency is observed around May 17th-18th, which coincides with a similar peak in the velocity ratio.
- Finally, the last peak in PV tendency, occurring on May 21st-22nd, is accompanied by a sharp increase in the ageostrophic-to-geostrophic velocity ratio, suggesting that intensified ageostrophic

contributions may be playing a role in disrupting PV conservation.

This alignment suggests that the increasing contribution of ageostrophic motion may be linked to the observed deviations in PV conservation, particularly in the second stage of the eddy's evolution. Additionally, the timeseries of H (fig. 4.3.10) also shows some correlation with the tendency of PV. When H remains constant, PV is approximately conserved, as indicated by relatively small fluctuations in PV tendency during the earlier phase of the eddy's evolution. However, starting from mid-May, the progressive reduction in H coincides with increasing deviations from PV conservation, as highlighted by the peaks in PV tendency. This suggests that as the eddy moves into shallower waters in mid-May, bathymetric constraints likely play a key role in modifying its structure. The minimum depth within the eddy's area decreases significantly (reaching values below 250 m, the estimated depth of eddy 1), which, in combination with the observed increase in PV tendency, suggests that the eddy is experiencing stronger bottom interactions. These interactions can induce bottom friction, enhance vertical mixing, and disrupt the coherence of the eddy structure, ultimately leading to energy dissipation. The simultaneous increase in ageostrophic motion further suggests a deviation from geostrophic balance, contributing to the eddy's instability. The correlation between PV tendency peaks and spikes in ageostrophic velocity reinforces the idea that non-conservative processes play a role in the eddy's weakening.
Overall, these findings indicate that the dissipation of eddy 1 results from a combination of bathymetric interaction and increasing ageostrophic effects. While the MFS model suggests its complete dissipation, SWOT observations indicate the pos-

sible formation of a new eddy in its place, underscoring the complexity of mesoscale dynamics in the region.

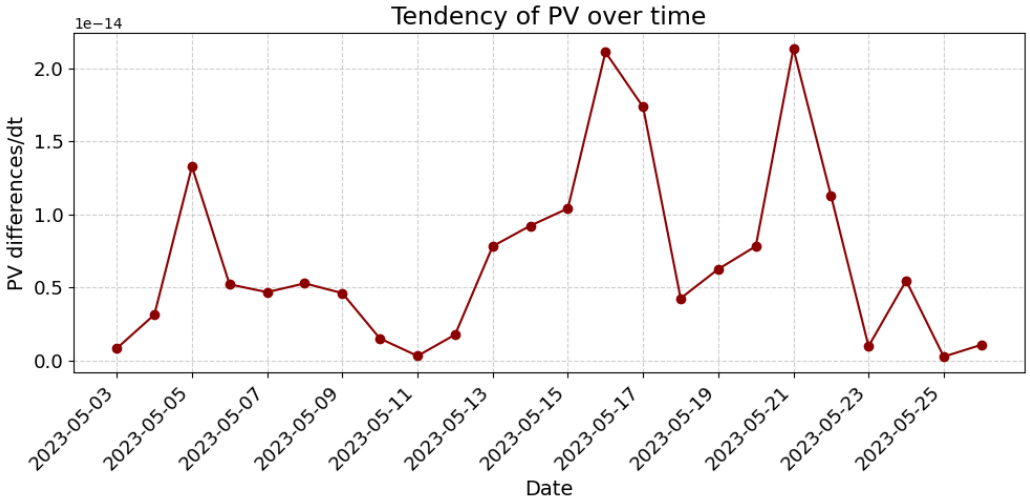

Figure 4.3.11: Tendency of potential vorticity over time.

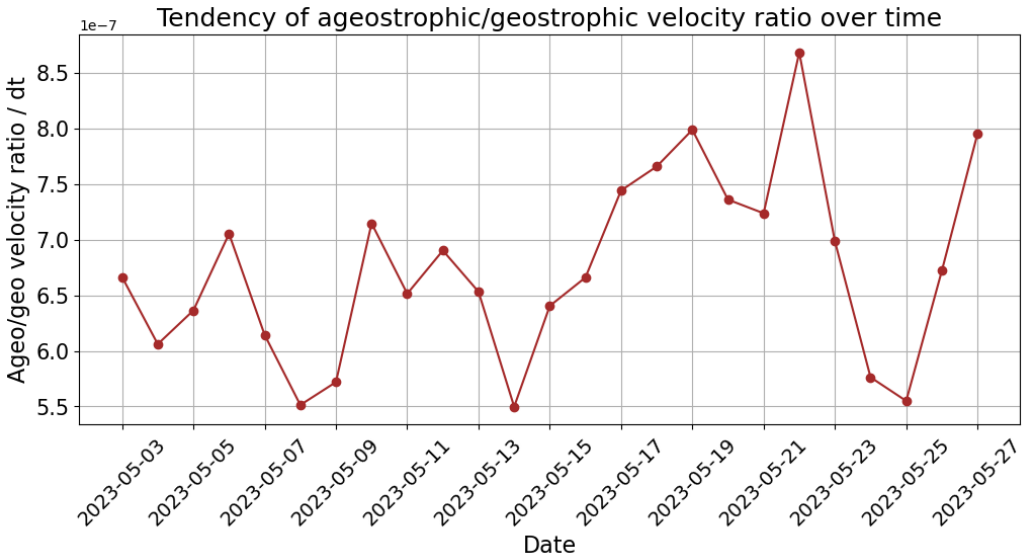

Figure 4.3.12: Tendency of ageostrophic/geostrophic velocity ratio over time.

Chapter 5

Conclusions

This study aimed to assess the added value of SWOT altimetry in resolving mesoscale eddies and their interactions with bathymetry, with a focus on eddy 1 in the Algerian Basin. The comparison between SWOT observations and conventional altimetry (L4 product), supported by numerical model data, allowed an evaluation of the ability of each dataset to capture eddy dynamics, including its propagation, evolution, and interaction with the seafloor.

The results indicate that SWOT provides a more detailed and accurate representation of eddy structures compared to conventional altimetry. Its higher spatial resolution allows for a sharper depiction of eddy boundaries and finer-scale variability, which are often smoothed out in gridded altimetric products. The comparison with independent datasets, such as sea surface temperature and chlorophyll-a concentration, further confirms the ability of SWOT to better align with observed oceanographic features. Additionally, the statistical validation of scale-dependent variability demonstrates that SWOT retains significantly more small-scale oceanic features than conventional altimetry, reinforcing its capability to resolve fine-scale processes.

One of the key aspects investigated in this study was eddy 1's evolution. We calculated the propagation velocity of the eddy with SWOT, conventional altimetry and model data, using three different methods: pyeddytracker algorithm, the smoothed coastline method, and SLA max tracking method. While some differences emerge depending on the dataset, the estimated speeds remain broadly consistent and in agreement with previous studies in the region.

A major finding of this study is the improved ability to track the final stages of eddy 1's evolution and dissipation. Conventional altimetry struggles to clearly distinguish its dissipation, likely due to interpolation artifacts, whereas SWOT and MFS model reveal a progressive weakening phase leading to the disappearance of the eddy. The complementary insights from SWOT and the model enabled the identification of a key dynamical feature: what initially appeared to be a single deformed structure was actually an eddy undergoing dissipation, followed by the formation of a new one. This distinction was not evident in conventional altimetry alone, highlighting the added value of SWOT's high-resolution observations in understanding mesoscale ocean dynamics.

The numerical model provided further insights into the mechanisms driving the evolution and dissipation of eddy 1. The model revealed that, as the eddy evolved, its relative vorticity exhibited a clear trend towards zero, particularly in the final phase before dissipation. This behavior is consistent with the shrinking of the eddy radius, inferred from its contour evolution. At the same time, potential vorticity deviations from its conservation became more pronounced in the last stage of propagation, particularly as the eddy encountered shallower bathymetry. The model also

highlighted an increase in the ageostrophic component of motion, indicating a progressive breakdown of geostrophic balance. These factors likely played a key role in weakening the eddy, ultimately leading to its dissipation. The model thus played a crucial role in diagnosing the interaction between the eddy and the bathymetry, a process that conventional altimetry alone could not resolve.

While this study demonstrates the advantages of SWOT altimetry in capturing mesoscale eddy dynamics, some limitations remain. The primary constraint of SWOT data is its swath-based sampling, which introduces data gaps and limits temporal continuity compared to conventional altimetry. This can affect the ability to track eddy evolution over extended periods, particularly in rapidly evolving regions where frequent observations are needed. Moreover, SWOT's observational record is still relatively short, restricting long-term statistical analyses of mesoscale variability.

Looking ahead, future studies could benefit from the integration of SWOT into operational oceanographic models, that could lead to improvements in the representation of mesoscale structures and their dissipation. The incorporation of in-situ measurements would provide valuable constraints on the vertical structure of eddies, improving estimates of their depth and stratification. While this study focused primarily on eddy 1, the methodological framework developed could be extended to investigate eddy 2. Future analysis could apply the same techniques to assess its evolution, providing an additional case study for evaluating SWOT's capabilities in resolving mesoscale dynamics. Furthermore, extending the analysis to additional SWOT cycles beyond the fast-sampling phase could offer insights into

seasonal and interannual eddy variability. Investigating submesoscale processes within SWOT's resolving range would also help refine our understanding of energy dissipation mechanisms and eddy life cycles.

Bibliography

G. Aulicino, Y. Cotroneo, S. Ruiz, A. Sánchez Román, A. Pascual, G. Fusco, J. Tintoré, and G. Budillon. Monitoring the Algerian Basin through glider observations, satellite altimetry and numerical simulations along a SARAL/AltiKa track. *Journal of Marine Systems*, 179:55–71, March 2018. ISSN 09247963. doi: 10.1016/j.jmarsys.2017.11.006. URL https://linkinghub.elsevier.com/retrieve/pii/S0924796317302658.

Mejdoub Benzohra and Claude Millot. Characteristics and circulation of the surface and intermediate water masses off Algeria. *Deep Sea Research Part I: Oceanographic Research Papers*, 42(10):1803–1830, October 1995. ISSN 0967-0637. doi: 10.1016/0967-0637(95)00043-6. URL https://www.sciencedirect.com/science/article/pii/0967063795000436.

Antonio Bonaduce, Andrea Cipollone, Johnny A. Johannessen, Joanna Staneva, Roshin P. Raj, and Ali Aydogdu. Ocean Mesoscale Variability: A Case Study on the Mediterranean Sea From a Re-Analysis Perspective. *Frontiers in Earth Science*, 9, September 2021. ISSN 2296-6463. doi: 10.3389/feart.2021.724879. URL https://www.frontiersin.org/journals/earth-science/

articles/10.3389/feart.2021.724879/full. Publisher: Frontiers.

B. Buongiorno Nardelli, C. Tronconi, A. Pisano, and R. Santoleri. High and Ultra-High resolution processing of satellite Sea Surface Temperature data over Southern European Seas in the framework of MyOcean project. *Remote Sensing of Environment*, 129:1–16, February 2013. ISSN 00344257. doi: 10.1016/j.rse.2012.10.012. URL https://linkinghub.elsevier.com/retrieve/pii/S003442571200394X.

Loren Carrere, Brian K. Arbic, Brian Dushaw, Gary Egbert, Svetlana Erofeeva, Florent Lyard, Richard D. Ray, Clément Ubelmann, Edward Zaron, Zhongxiang Zhao, Jay F. Shriver, Maarten Cornelis Buijsman, and Nicolas Picot. Accuracy assessment of global internal-tide models using satellite altimetry. *Ocean Science*, 17(1):147–180, January 2021. ISSN 1812-0784. doi: 10.5194/os-17-147-2021. URL https://os.copernicus.org/articles/17/147/2021/. Publisher: Copernicus GmbH.

Loren Carrere, Florent Lyard, Mathilde Cancet, Damien Allain, Mei-Ling Dabat, Ergane Fouchet, Etienne Sahuc, Yannice Faugere, Gerald Dibarboure, and Nicolas Picot. *A new barotropic tide model for global ocean: FES2022*. October 2022. doi: 10.24400/527896/a03-2022.3287. URL https://ui.adsabs.harvard.edu/abs/2022osts.confE..43C. Conference Name: 2022 Ocean Surface Topography Science Team Meeting Pages: 43 ADS Bibcode: 2022osts.confE..43C.

Dudley B. Chelton, Peter Gaube, Michael G. Schlax, Jeffrey J. Early, and Roger M. Samelson. The Influence of Nonlinear Mesoscale Eddies on Near-Surface Oceanic Chlorophyll.

Science, 334(6054):328–332, October 2011. doi: 10.1126/science.1208897. URL https://www.science.org/doi/10.1126/science.1208897. Publisher: American Association for the Advancement of Science.

E. Clementi, J. Pistoia, D. Delrosso, G. Mattia, C. Fratianni, A. Storto, S. Ciliberti, B. Lemieux, E. Fenu, S. Simoncelli, M. Drudi, A. Grandi, D. Padeletti, P. Di Pietro, and N. Pinardi. A 1/24° resolution Mediterranean physical analysis and forecasting system for the Copernicus Marine Environment Monitoring Service. 2018. ISBN 978-2-9601883-3-2. URL https://cris.unibo.it/handle/11585/674917.

Francesco d'Ovidio, Ananda Pascual, Jinbo Wang, Andrea M. Doglioli, Zhao Jing, Sebastien Moreau, Gérald Grégori, Sebastiaan Swart, Sabrina Speich, Frédéric Cyr, Benoit Legresy, Yi Chao, Lee Fu, and Rosemary Anne Morrow. Frontiers in Fine-Scale in situ Studies: Opportunities During the SWOT Fast Sampling Phase. *Frontiers in Marine Science*, 6:168, April 2019. ISSN 2296-7745. doi: 10.3389/fmars.2019.00168. URL https://www.frontiersin.org/article/10.3389/fmars.2019.00168/full.

Romain Escudier. EDDIES IN THE WESTERN MEDITERRANEAN SEA: CHARACTERIZATION AND UNDERSTANDING FROM SATELLITE OBSERVATIONS AND MODEL SIMULATIONS. 2014.

Romain Escudier, Baptiste Mourre, Mélanie Juza, and Joaquín Tintoré. Subsurface circulation and mesoscale variability in the Algerian subbasin from altimeter-derived eddy trajectories. *Journal of Geophysical Research: Oceans*, 121(8):6310–6322, August 2016. ISSN 2169-9275, 2169-9291. doi: 10.1002/

2016JC011760. URL https://agupubs.onlinelibrary.wiley.com/doi/10.1002/2016JC011760.

Jordi Font, Jordi Isern-Fontanet, and José De Jesus Salas. Tracking a big anticyclonic eddy in the western Mediterranean Sea. *Scientia Marina*, 68(3):331–342, September 2004. ISSN 1886-8134, 0214-8358. doi: 10.3989/scimar.2004.68n3331. URL http://scientiamarina.revistas.csic.es/index.php/scientiamarina/article/view/379/380.

Lee-Lueng Fu, Dudley Chelton, Pierre-Yves Le Traon, and Rosemary Morrow. Eddy Dynamics From Satellite Altimetry. *Oceanography*, 23(4):14–25, December 2010. ISSN 10428275. doi: 10.5670/oceanog.2010.02. URL https://tos.org/oceanography/article/eddy-dynamics-from-satellite-altimetry.

Lee-Lueng Fu, Douglas Alsdorf, Rosemary Morrow, Ernesto Rodriguez, and Nelly Mognard. Wide-Swath Altimetric Measurement of Water Elevation on Earth. 2012.

Lee-Lueng Fu, Tamlin Pavelsky, Jean-Francois Cretaux, Rosemary Morrow, J. Thomas Farrar, Parag Vaze, Pierre Sengenes, Nadya Vinogradova-Shiffer, Annick Sylvestre-Baron, Nicolas Picot, and Gerald Dibarboure. The Surface Water and Ocean Topography Mission: A Breakthrough in Radar Remote Sensing of the Ocean and Land Surface Water. *Geophysical Research Letters*, 51(4):e2023GL107652, February 2024. ISSN 0094-8276, 1944-8007. doi: 10.1029/2023GL107652. URL https://agupubs.onlinelibrary.wiley.com/doi/10.1029/2023GL107652.

Giannetta Fusco, Vincenzo Artale, Yuri Cotroneo, and Gianmaria Sannino. Thermohaline variability of Mediterranean Water in the Gulf of Cadiz, 1948–1999. *Deep Sea Research Part I: Oceanographic Research Papers*, 55(12):1624–1638, December 2008. ISSN 09670637. doi: 10.1016/j.dsr.2008.07.009. URL https://linkinghub.elsevier.com/retrieve/pii/S0967063708001623.

M. Susan Lozier. Deconstructing the Conveyor Belt. *Science*, 328(5985):1507–1511, June 2010. ISSN 0036-8075, 1095-9203. doi: 10.1126/science.1189250. URL https://www.science.org/doi/10.1126/science.1189250.

Evan Mason, Ananda Pascual, and James C. McWilliams. A New Sea Surface Height–Based Code for Oceanic Mesoscale Eddy Tracking. May 2014. doi: 10.1175/JTECH-D-14-00019.1. URL https://journals.ametsoc.org/view/journals/atot/31/5/jtech-d-14-00019_1.xml. Section: Journal of Atmospheric and Oceanic Technology.

Claude Millot. Some features of the Algerian Current. *Journal of Geophysical Research: Oceans*, 90(C4):7169–7176, July 1985. ISSN 0148-0227. doi: 10.1029/JC090iC04p07169. URL https://agupubs.onlinelibrary.wiley.com/doi/10.1029/JC090iC04p07169.

Claude Millot. Circulation in the Western Mediterranean Sea. *Journal of Marine Systems*, 20(1-4):423–442, April 1999. ISSN 09247963. doi: 10.1016/S0924-7963(98)00078-5. URL https://linkinghub.elsevier.com/retrieve/pii/S0924796398000785.

Rosemary Morrow, Lee-Lueng Fu, Fabrice Ardhuin, Mounir

Benkiran, Bertrand Chapron, Emmanuel Cosme, Francesco d'Ovidio, J. Thomas Farrar, Sarah T. Gille, Guillaume Lapeyre, Pierre-Yves Le Traon, Ananda Pascual, Aurélien Ponte, Bo Qiu, Nicolas Rascle, Clement Ubelmann, Jinbo Wang, and Edward D. Zaron. Global Observations of Fine-Scale Ocean Surface Topography With the Surface Water and Ocean Topography (SWOT) Mission. *Frontiers in Marine Science*, 6:232, May 2019. ISSN 2296-7745. doi: 10.3389/fmars.2019.00232. URL https://www.frontiersin.org/article/10.3389/fmars.2019.00232/full.

D Obaton, C Millot, G Chabert D'Hières, and I Taupier-Letage. The Algerian current: comparisons between in situ and laboratory data sets. *Deep Sea Research Part I: Oceanographic Research Papers*, 47(11):2159–2190, November 2000. ISSN 0967-0637. doi: 10.1016/S0967-0637(00)00014-5. URL https://www.sciencedirect.com/science/article/pii/S0967063700000145.

Federica Pessini, Antonio Olita, Yuri Cotroneo, and Angelo Perilli. Mesoscale eddies in the Algerian Basin: do they differ as a function of their formation site? *Ocean Science*, 14(4):669–688, July 2018. ISSN 1812-0792. doi: 10.5194/os-14-669-2018. URL https://os.copernicus.org/articles/14/669/2018/.

N. Pinardi and G. Coppini. Preface "Operational oceanography in the Mediterranean Sea: the second stage of development". *Ocean Science*, 6(1):263–267, February 2010. ISSN 1812-0792. doi: 10.5194/os-6-263-2010. URL https://os.copernicus.org/articles/6/263/2010/.

N. Pinardi and E. Masetti. Variability of the large scale general circulation of the Mediterranean Sea from observations and modelling: a review. *Palaeogeography, Palaeoclimatology, Palaeoecology*, 158(3-4):153–173, May 2000. ISSN 00310182. doi: 10.1016/S0031-0182(00)00048-1. URL https://linkinghub.elsevier.com/retrieve/pii/S0031018200000481.

N. Pinardi, E. Demirov, M. Tonani, L. Giacomelli, C. Fratianni, and MFSPP partners. Mediterranean ocean forecasting system: First phase of implementation. In N. C. Fiemming, S. Vallerga, N. Pinardi, H. W. A. Behrens, G. Manzella, D. Prandle, and J. H. Stei, editors, *Elsevier Oceanography Series*, volume 66 of *Opertional Oceanography*, pages 189–197. Elsevier, January 2002. doi: 10.1016/S0422-9894(02)80023-X. URL https://www.sciencedirect.com/science/article/pii/S042298940280023X.

Pierre-Marie Poulain, Luca Centurioni, Tamay Özgökmen, Daniel Tarry, Ananda Pascual, Simon Ruiz, Elena Mauri, Milena Menna, and Giulio Notarstefano. On the Structure and Kinematics of an Algerian Eddy in the Southwestern Mediterranean Sea. *Remote Sensing*, 13(15):3039, August 2021. ISSN 2072-4292. doi: 10.3390/rs13153039. URL https://www.mdpi.com/2072-4292/13/15/3039.

M.-H. Rio, A. Pascual, P.-M. Poulain, M. Menna, B. Barceló, and J. Tintoré. Computation of a new mean dynamic topography for the Mediterranean Sea from model outputs, altimeter measurements and oceanographic in situ data. *Ocean Science*, 10(4):731–744, August 2014. ISSN 1812-0784. doi:

10.5194/os-10-731-2014. URL https://os.copernicus.org/articles/10/731/2014/. Publisher: Copernicus GmbH.

A.R. Robinson, W.G. Leslie, A. Theocharis, and A. Lascaratos. Mediterranean Sea Circulation. In *Encyclopedia of Ocean Sciences*, pages 1689–1705. Elsevier, 2001. ISBN 978-0-12-227430-5. doi: 10.1006/rwos.2001.0376. URL https://linkinghub.elsevier.com/retrieve/pii/B012227430X003767.

S Ruiz, J Font, M Emelianov, J Isern-Fontanet, C Millot, J Salas, and I Taupier-Letage. Deep structure of an open sea eddy in the Algerian Basin. *Journal of Marine Systems*, 33-34:179–195, June 2002. ISSN 09247963. doi: 10.1016/S0924-7963(02)00058-1. URL https://linkinghub.elsevier.com/retrieve/pii/S0924796302000581.

Detlef Stammer, Claus Böning, and Christian Dieterich. The role of variable wind forcing in generating eddy energy in the North Atlantic. *Progress in Oceanography*, 48(2):289–311, January 2001. ISSN 0079-6611. doi: 10.1016/S0079-6611(01)00008-8. URL https://www.sciencedirect.com/science/article/pii/S0079661101000088.

P. Testor, U. Send, J.-C. Gascard, C. Millot, I. Taupier-Letage, and K. Béranger. The mean circulation of the southwestern Mediterranean Sea: Algerian Gyres. *Journal of Geophysical Research: Oceans*, 110(C11):2004JC002861, November 2005. ISSN 0148-0227. doi: 10.1029/2004JC002861. URL https://agupubs.onlinelibrary.wiley.com/doi/10.1029/2004JC002861.

Zhengguang Zhang, Wei Wang, and Bo Qiu. Oceanic mass

transport by mesoscale eddies. *Science*, 345(6194):322–324, July 2014. ISSN 0036-8075, 1095-9203. doi: 10.1126/science.1252418. URL https://www.science.org/doi/10.1126/science.1252418.